Article

# First-in-human study of epidural spinal cord stimulation in individuals with spinal muscular atrophy

Genís Prat-Ortega [1,2,18], Scott Ensel[2,3,18], Serena Donadio[1,2,3,18], Luigi Borda [4,5], Amy Boos[2,6], Prakarsh Yadav[4,5], Nikhil Verma [4,5], Jonathan Ho[1,2], Erick Carranza[2,3], Sarah Frazier-Kim [1,2], Daryl P. Fields[1,2], Lee E. Fisher [2,3,7,8], Doug J. Weber [4,5,9], Jeffrey Balzer[1], Tina Duong[10], Steven D. Weinstein[11], Mikael J. L. Eliasson[11], Jacqueline Montes [12], Karen S. Chen[13], Paula R. Clemens [6], Peter Gerszten[1], George Z. Mentis[14,15,16], Elvira Pirondini [2,3,7,17,19] ✉, Robert M. Friedlander [1,19] ✉ & Marco Capogrosso [1,2,3,19] ✉

Spinal muscular atrophy (SMA) is an inherited neurodegenerative disease causing motoneuron dysfunction, muscle weakness, fatigue and early mortality. Three new therapies can slow disease progression, enabling people to survive albeit with lingering motor impairments. Indeed, weakness and fatigue are still among patients' main concerns. Here we show that epidural spinal cord stimulation (SCS) improved motoneuron function, thereby increasing strength, endurance and gait quality, in three adults with type 3 SMA. Preclinical works demonstrated that SMA motoneurons show low firing rates because of a loss of excitatory input from primary sensory afferents. In the present study, we hypothesized that correcting this loss with electrical stimulation of the sensory afferents could improve motoneuron function. To test this hypothesis, we implanted three adults with SMA with epidural electrodes over the lumbosacral spinal cord, targeting sensory axons of the legs. We delivered SCS for 4 weeks, 2 h per day during motor tasks. Our intervention led to improvements in strength (up to +180%), gait quality (mean step length: +40%) and endurance (mean change in 6-minute walk test: +26 m), paralleled by increased motoneuron firing rates. These changes persisted even when SCS was turned OFF. Notably, no adverse events related to the stimulation were reported. ClinicalTrials.gov identifier: NCT05430113.

Onset and progression in neurodegenerative diseases are commonly assumed to be driven by progressive neuronal death, leading to cognitive and motor impairments[1–7]. In fact, in addition to neuronal death, synaptic circuit dysfunction is emerging as another determinant of deficits in Parkinson's disease, Alzheimer's disease, Huntington's disease, amyotrophic lateral sclerosis and SMA[8–12]. Therefore, targeting neuronal death is not sufficient to reverse the disease phenotype. Instead, attention must be brought to the design of therapies that also target

neural circuit dysfunction. Given the existence of neuroprotective therapies for SMA[13] and the basic circuits affected[12], SMA is particularly suited to validate a combined disease-modifying strategy targeting neuroprotection and improvement of neural circuit function. SMA is an inherited spinal motor circuit disorder caused by the homozygous loss of the *SMN1* gene, which results in ubiquitous deficits of SMN protein expression[14,15]. Lack of SMN leads to selective death of spinal motoneurons and progressive muscle atrophy. SMA manifests with
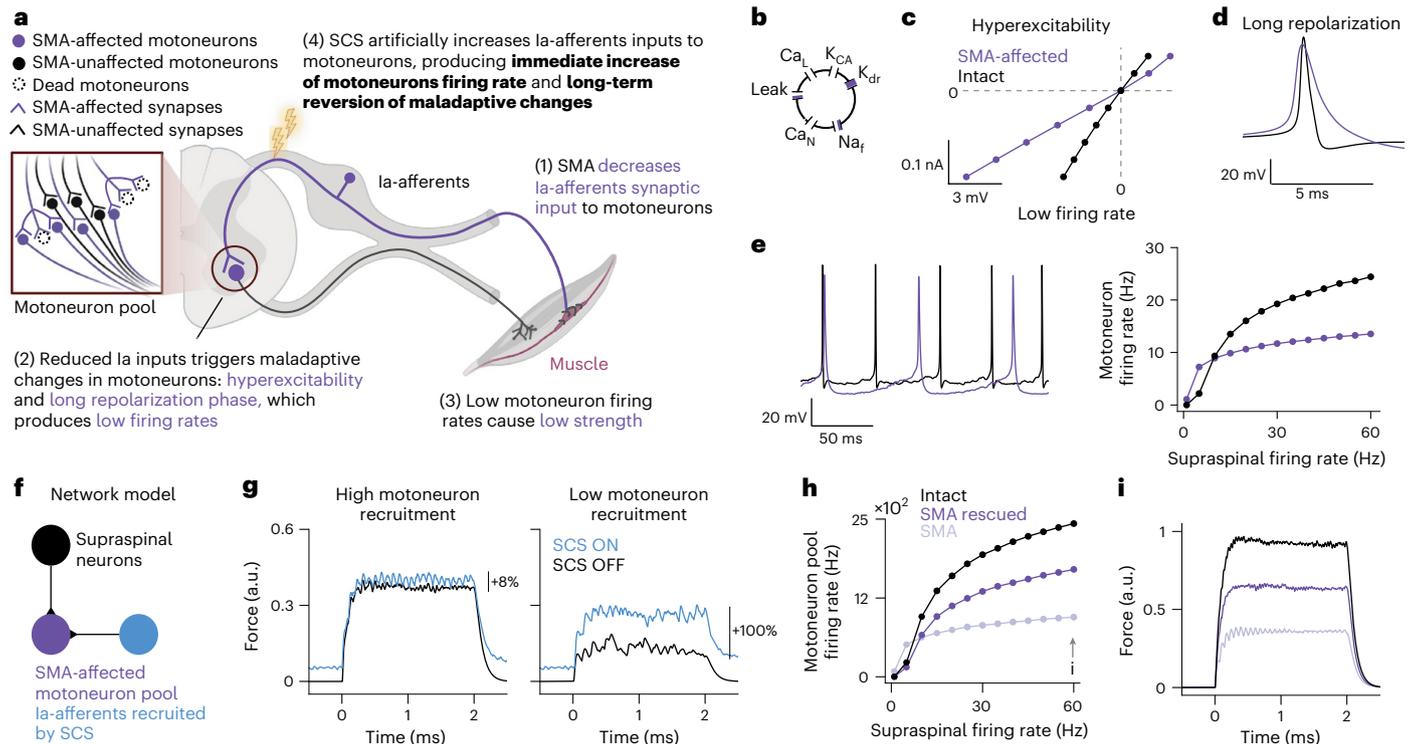
Fig. 1 | Hypothesis and theoretical framework. a, Study hypothesis.
b, A Hodgkin–Huxley model with an almost complete blocked delayed rectifier and partially blocked sodium and leak channels. **c**–**e**, Reproduced electrical properties of SMA-affected motoneurons[18]: hyperexcitability characterized by a higher input resistance (**c**), longer repolarization phase following an action potential (**d**) and lower firing rate (**e**). **f**, Network model schema: the SMA-affected motoneuron pool receives excitatory inputs from supraspinal neurons and Ia-afferents recruited by SCS. **g**, Assistive effect. Simulated force produced by an SMA-affected motoneuron pool with 30% motoneuron loss and 50% SMA-affected motoneurons with and without SCS. SCS amplitude: 11 Ia-afferents recruited;

SCS frequency: 40 Hz. The magnitude of the assistive effects depended on the recruitment of the motoneuron pool. With high motoneuron recruitment (supraspinal firing rate of 20 Hz), SCS resulted in only 8% increase in torque, whereas, with low motoneuron recruitment (supraspinal firing rate of 5 Hz), SCS led to a 100% increase in torque. **h,i**, Therapeutic effect. Simulated firing rates (**h**) and forces (**i**) for a motoneuron pool with 30% of motoneuron loss. The biophysical model predicted a large increase of maximum firing rate and force when SMA-affected motoneurons are functionally rescued. However, the maximum force was still affected by motoneuron death. Created in BioRender: Donadio, S. (2024), https://BioRender.com/g49q959.

varying phenotypic severities that depend on the number of copies of the nearly identical *SMN2* gene and range from premature infant death (type 1) to normal lifespan adults (type 3) living with progressive motor deficits and disability[16]. In the past 7 years, three breakthrough therapeutics that upregulate the synthesis of SMN were approved, revolutionizing clinical care of SMA[13]. However, although these therapies effectively prevent mortality of affected children and decelerate disease progression in adults, they have proven ineffective in completely reversing motor deficits. Consequently, treated individuals exhibit persistent impairments throughout development and into adulthood and indicate weakness and fatigue as primary concerns[17]. This situation stems from the fact that motor deficits in SMA are not exclusively caused by motoneuron death. Animal models of SMA show that motor deficits appear before widespread motoneuron death[12], suggesting that spinal circuit dysfunction may play a role in disease onset and progression. Importantly, excitatory synaptic input to spinal motoneurons coming from proprioceptive afferents is lower in SMA[12,18]. In turn, this excitatory deficiency causes SMA-affected motoneurons to homeostatically compensate by altering membrane ion channel densities[18,19]. Unfortunately, these maladaptive changes lead to hyperexcitable motoneurons that are paradoxically incapable of producing sustained action potential firing and, consequently, normal muscle contraction[18,20] even after the administration of SMN-inducing therapies[18] (Fig. 1a).

Upregulating the activity of primary sensory afferents could compensate for the loss of excitatory input to motoneurons, potentially triggering circuit dysfunction reversal[20] (Fig. 1a). We, therefore, sought

to achieve selective upregulation of spinal sensory afferents in humans by means of electrical stimulation. We used spinal cord stimulation (SCS), a clinically approved neurostimulation technology[21], to activate sensory afferents in the posterior roots[22,23]. Using SCS, we tested two hypotheses: (1) when turned ON, SCS can increase motoneuron firing rates, thereby immediately increasing strength and quality of movement—an assistive effect (that is, an effect that is immediate; it assists movement but disappears when SCS is turned OFF); and (2), over time, SCS would lead to the reversal of maladaptive changes in the electrical properties of SMA-affected motoneurons, thereby mitigating motor deficits in humans—a therapeutic effect (that is, an effect that persists when SCS is OFF).

Results

Does known biophysics support the use of SCS in SMA?

We first investigated whether motoneuron function could be improved by SCS using computational biophysics[22–27]. Specifically, we created a Hodgkin–Huxley-based model of SMA-affected motoneurons[25,27,28] that reproduce the biophysical signatures of SMA dysfunction: hyperexcitability, low firing rates and decreased synaptic inputs from Ia-afferents[12,18]. Specifically, we adjusted ion conductances to mimic passive and active hyperexcitability of SMA-affected motoneurons (Fig. 1b,c and Extended Data Fig. 1a,b). Following data in mice[18], we reduced the delayed rectifier potassium channel conductance, which extended action potential duration and reduced firing rates[18] (Fig. 1d,e and Supplementary Methods). Finally, we reduced the strength of Ia-afferents synapses[18].

Experimental data show that surviving motorpools in SMA are composed of a mix of normal functioning units (SMA-unaffected) and dysfunctional units (SMA-affected)[12,18]. Thus, we simulated an SMA-affected motoneuron pool by (1) reducing the number of motoneurons and (2) mixing SMA-affected and SMA-unaffected motoneurons. The motoneuron pool received inputs from supraspinal neurons (to mimic volitional recruitment) and sensory afferents recruited with SCS (Fig. 1f and Extended Data Fig. 1c). As expected, when simulating volitional force production, our model produced markedly lower forces than a fully-intact motoneuron population (Extended Data Fig. 1d,e).

We then checked if SCS could yield beneficial strength assistance in SMA (hypothesis 1). For this, we modeled the effects of SCS as a synchronous activation of Ia-afferents at the stimulation frequency[22,25–27] (Fig. 1f and Extended Data Fig. 1c). When SCS was turned ON (40 Hz), motoneurons produced higher firing rates that translated into higher simulated forces compared to SCS OFF (Fig. 1g and Extended Data Fig. 1f,g). However, these gains were higher at lower forces (+100%; that is, when fewer motoneurons were active) than at higher forces (+10%). In other words, if all motoneurons were volitionally recruited at their maximum firing rates, SCS could not further increase their firing rates (Extended Data Fig. 1f,g). Thus, our model predicts that SCS should be able to immediately increase motoneuron firing rates in SMA; however, the magnitude of this assistive effect would depend on the exerted effort. Specifically, SCS should be more effective during lower-effort activities than during maximum voluntary muscle contraction.

Our second hypothesis is that applying SCS over time could reverse motoneuron dysfunction by compensating for its underlying cause: the reduction in excitatory sensory input[18]. This rescue would result in an increase in motoneuron firing capacity over time, even in the absence of SCS, demonstrating a therapeutic effect (Fig. 1a). Therefore, we studied the effect that rescuing some of the SMA-affected motoneurons (that is, transforming SMA-affected into SMA-unaffected motoneurons) would have on simulated forces. We found that rescuing the function of SMA-affected motoneurons in our model led to improvements in strength (Fig. 1h,i and Extended Data Fig. 1h,i) that were much larger than the assistive effects of SCS.

In summary, our model predicted that (1) SCS should assist in generating movement when ON (assistive effects) and (2) if SCS could rescue the function of some SMA-affected neurons, it would lead to even higher improvements in strength (therapeutic effects).

Exploratory clinical study design

To test our hypotheses, we conducted a first-in-human study (NCT05430113) in ambulatory adults with SMA (type 3 phenotype), assessing the feasibility of using SCS to improve leg motor function. The study was approved by the University of Pittsburgh institutional review board (IRB, n21080158). We recruited three participants with lower-limb weakness who were able to stand and walk: SMA01 (Hispanic male, 22 years old, four *SMN2* copies, no SMN treatment, enrollment Hammersmith Functional Motor Scale Expanded (HFMSE): 60/66 points); SMA02 (white male, 55 years old, four *SMN2* copies, treated with nusinersen, enrollment HFMSE: 40/66 points); and SMA03 (white male, 30 years old, four *SMN2* copies, treated with nusinersen, enrollment HFMSE: 49/66 points) (Extended Data Fig. 2a,d,g and Methods). Participants received a temporary implant of two (one per side) eight-contact linear epidural leads for 29 days (after which the leads were removed; Fig. 2a). Using intraoperative mapping[29,30], we positioned the leads above spinal segments L1–S1 to engage the posterior roots innervating leg muscles[29] (Fig. 2a and Extended Data Fig. 2b,e,h). After recovery, participants underwent 19 sessions of walking, muscle strength, endurance and electrophysiology assessments geared to quantify the assistive and therapeutics effects of SCS as well as to validate its mechanisms of action (Fig. 2b,c). Assessments included 3D kinematics during walking,
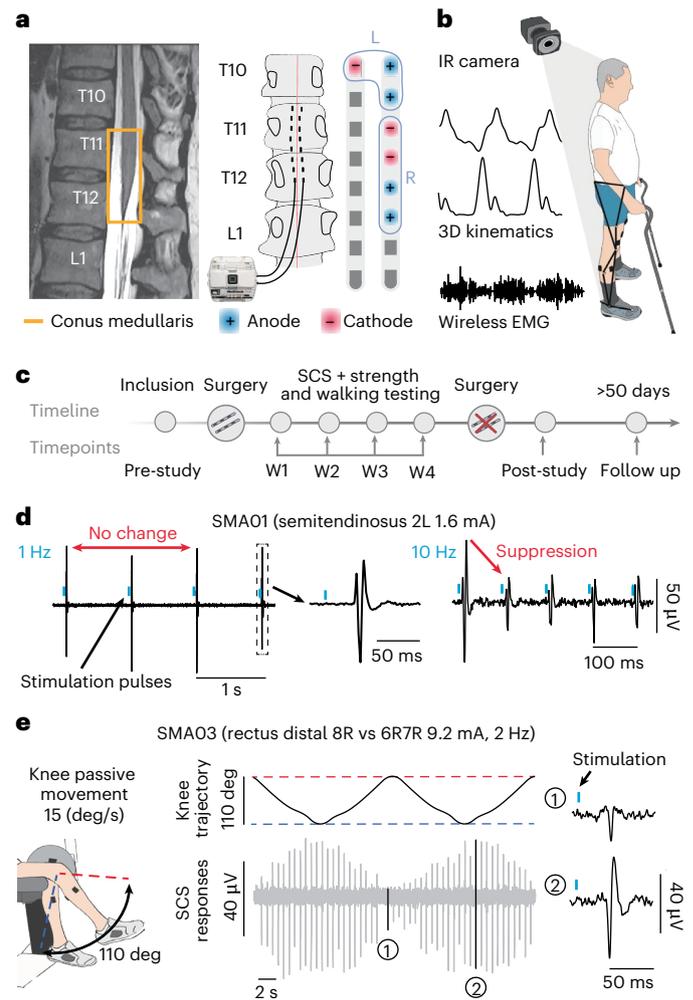
Fig. 2 | Study design and evidence for sensory recruitment with SCS. a, Left, example of T2 MRI (SMA02)—the conus medullaris (highlighted in yellow) is located under the T12 vertebra. Center, the electrodes were bilaterally placed in the epidural space. For SMA02, they were placed between T11 and T12. In most of the experiments, we used a wireless stimulator connected to the leads with eight contacts each. Right, example of SCS parameters (SMA03), where we used a program targeting the right (amplitude: 5 mA; frequency: 40 Hz; pulse width: 400 µs) and the left (amplitude: 5.5 mA; frequency: 40 Hz; pulse width: 400 µs) leg hip flexors and knee extensor muscles. **b**, We recorded 3D kinematics and EMG activity bilaterally of seven different muscles (semitendinosus (ST); bicep femoris (BF); vastus lateralis (VL); rectus femoris proximal (RP); rectus femoris distal (RD); gastrocnemius (G); tibialis anterior (TA)) during overground walking. **c**, Study timeline. **d**, Example of frequency-dependent suppression (SMA01). We observed decreased peak-to-peak responses as we increased the frequency of single SCS pulses, indicating the sensory-driven recruitment of motoneurons. **e**, Left, example setup for passive knee joint movement (SMA03). The participants were secured to a robotic system that moved the knee joint passively within the reported ROM. SCS parameters were configured to target a muscle that underwent stretching cycles during the joint movement. Center, joint angles during the 110° oscillation and the corresponding EMG activity of the rectus femoris. Spinal reflexes are clearly modulated by joint angles, indicating that SCS activates sensory afferents. Insets 1 and 2 show two spinal reflex examples at maximum knee extension and flexion, respectively. Created in BioRender: Donadio, S. (2024), https://BioRender.com/d20k890. deg, degrees; IR, infrared; W, week.

electromyography (EMG), single joint isometric torques, transcranial magnetic stimulation (TMS) and functional magnetic resonance imaging (fMRI) of the spinal cord[31]. We individualized SCS parameters to target the hip and knee muscles (most affected in SMA), following our
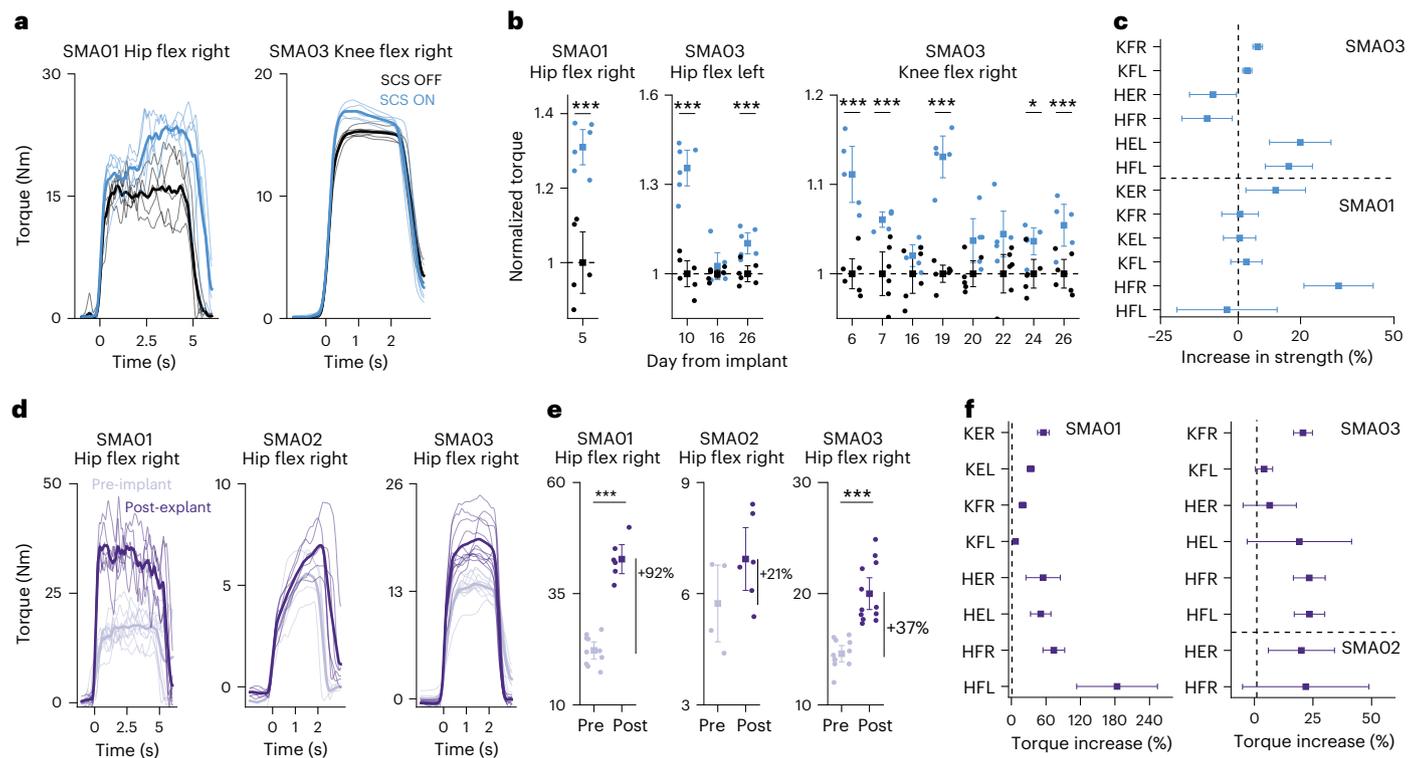
Fig. 3 | SCS improves muscle strength. a, Examples of isometric torque traces during maximum voluntary contraction (MVC) with and without SCS; light lines correspond to single trials, whereas thick lines are the means across trials. **b**, Maximum torque for SCS ON and OFF. Each repetition (single dots) was normalized by the mean SCS OFF maximum torque of each session. **c**, Mean assistive increase in strength across days (SCS ON versus OFF, same day) for all muscles and participants that we could reliably measure (torques above 4 Nm). We noticed that SMA01 improved in his right knee especially when he was already fatigued. **d**, Example of isometric torque traces during MVC of the hip flexion

right pre-implant and post-explant without SCS for all participants. **e**, Maximum torque produced for hip flexion right for all participants pre-implant and post-explant (post-explant, 4 or 5 days after the explant). Each dot represents a repetition. **f**, Therapeutic increases in strength for all muscles and participants that we could reliably measure (torques above 4 Nm). See Extended Data Fig. 3 for the significance tests of all muscles. All error bars indicate the mean and 95% CI of the mean, computed with bootstrapping ($n = 10,000$). Statistical significance was assessed with two-sided bootstrapping ($n = 10,000$): $*P < 0.05$, $**P < 0.01$, $***P < 0.001$. E, extension; F, flexion; H, hip; K, knee; L, left; R, right.

protocolled approach[29,30,32] (Supplementary Methods), and used these configurations for the rest of the study (Fig. 2a and Extended Data Fig. 2c,f,i). Notably, no adverse events related to the use of SCS in SMA were reported (see detailed list in the Supplementary Information).

SCS does not directly stimulate motoneurons in SMA

In humans, SCS recruits motoneurons indirectly via the recruitment of the sensory afferents in the posterior roots[22,23,29,30,33]. However, given the degeneration of circuits in SMA, we sought to verify that SCS stimulated the sensory afferents also in SMA with three experiments. First, we checked for rate-dependent depression (RDD), a signature of sensory-mediated recruitment of motoneurons[30,34–37]. EMG responses evoked by single pulses of SCS were suppressed at higher SCS frequencies (>10 Hz) (Fig. 2d), which confirmed RDD. Second, we verified that the amplitude of evoked reflex responses was dependent on joint angles, an additional signature of sensory-driven recruitment of motoneurons[25]. We measured peak-to-peak EMG responses evoked by each SCS pulse during passive motion of the leg at controlled speed (CSMi, HUMAC NORM) and found clear joint angle dependencies (Fig. 2e, Extended Data Fig. 2j–p and Supplementary Methods). Finally, we measured proprioception acuity by passively moving participants' legs and asked them to identify the instant at which they detected movement (blindfolded and acoustically isolated[25] (Supplementary Methods). In all three participants, high-stimulation amplitudes increased the time at which participants perceived movement (Extended Data Fig. 2q,r), demonstrating a disruption of movement perception caused by stimulation of the afferents.

Effects of SCS on muscle strength

We quantified the assistive effects of SCS on strength by comparing isometric torques during maximal voluntary contractions at the hip and knee joints (Fig. 3a–c) with and without SCS. We analyzed all joints where participants could produce more than 4 Nm (above system mechanical noise; Methods and Extended Data Figs. 3 and 4). All participants had substantial leg muscle weakness (up to 220 times weaker than able-bodied persons[38]). When SCS was turned ON (motor threshold, 40 Hz), we observed facilitation in all joints (that is, extension or flexion: up to +31%, SCS OFF: 19.8 Nm, 95% confidence interval (CI): (18.2, 21.4), SCS ON: 25.9 Nm, 95% CI: (25, 26.9) in SMA01 right hip flexion; Fig. 3a–c and Extended Data Figs. 3b and 4h–j) but not all functions (this may be caused by lack of specificity of the stimulation). Participants reported that movements felt easier when SCS was ON. Because they could always feel that SCS was active[30], we could not execute a blinded control; however, they were not able to distinguish among different SCS parameters. Therefore, we executed sham controls by changing SCS parameters without participant knowledge and demonstrated that the effects vanished for non-optimal SCS parameters[30] (Extended Data Fig. 5d,e).

Notably, we found large improvements that emerged over time with SCS OFF in almost all leg muscles (13/16) (Fig. 3d–f and Extended Data Fig. 3a), and particularly at the hip flexors (Fig. 3d,e), in all participants (up to +180%, from 18.4 Nm, 95% CI: (17.7, 19.1) pre-implant to 52.2 Nm, 95% CI: (39.4, 64.6) post-explant in left hip flexion for SMA01). These therapeutic improvements exceed in size the assistive effects and led to substantial motor benefits. For example, with assistive effects
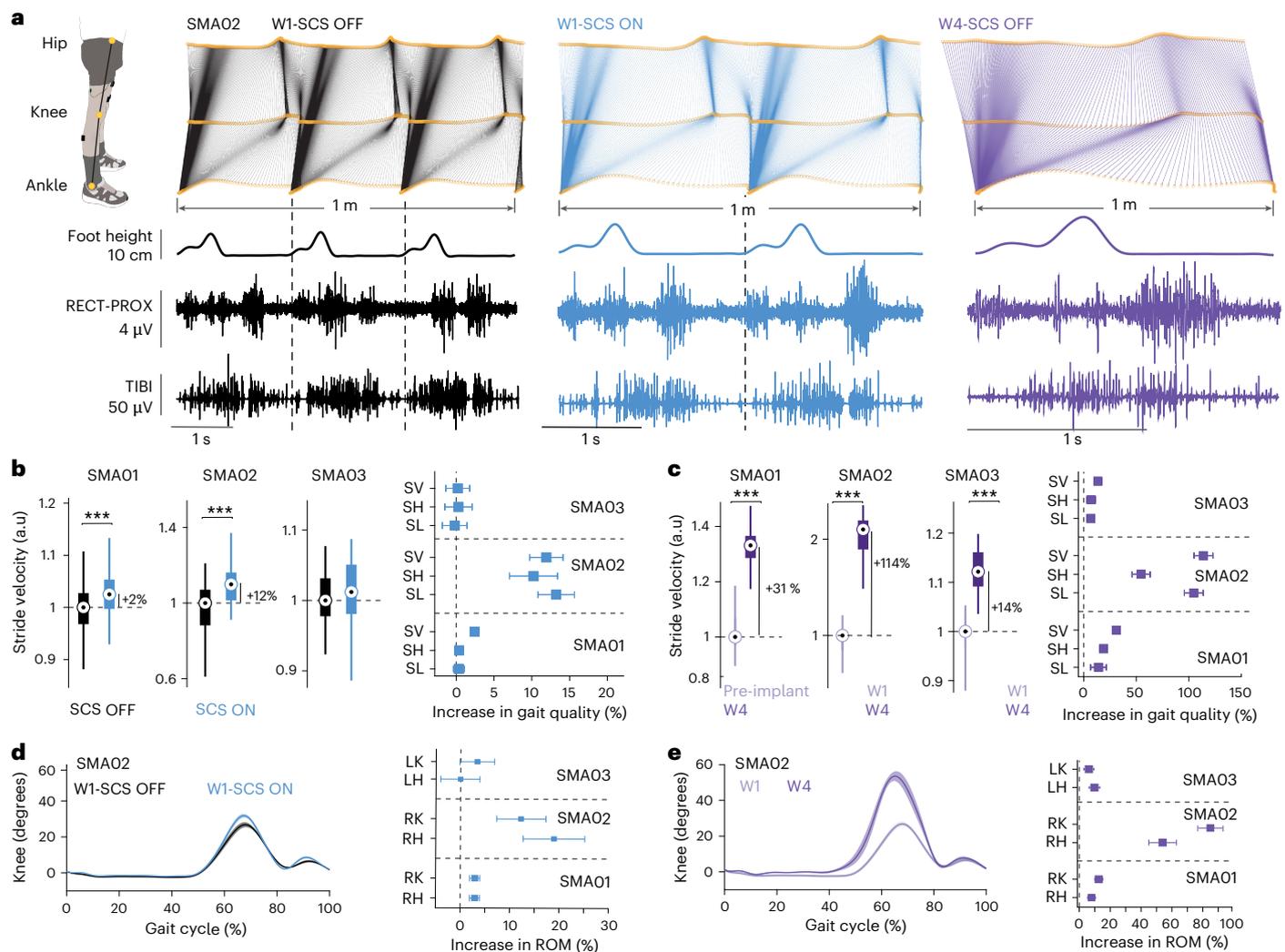
Fig. 4 | SCS improves gait quality. a, Example of the walking pattern (stick diagrams; SMA02) across a fixed distance under varying conditions: week 1 SCS OFF (black) and SCS ON (light blue) and week 4 SCS OFF (purple). Bottom, foot height and EMG activity for the rectus femoris proximal (RECT-PROX) and tibialis anterior (TIBI) during the same distance walked. To cover 1 m, SMA02 needed three strides in week 1, two strides in week 1 with SCS ON and only one stride in week 4 with SCS OFF. **b**, Left, stride velocity (SV) with and without stimulation for all participants. Right, mean and 95% CI of the change in gait quality variables (step length (SL), step height (SH) and stride velocity (SV)) with and without SCS for all participants. **c**, As in **b** for the therapeutic effects (SCS OFF first versus last overground walking sessions). **d**, Left, percentage assistive increase in hip and knee ROM for all participants. Right, mean and 95% CI of knee ROM throughout the gait cycle with and without SCS in week 1 (assistive effect). **e**, As in **b** but comparing weeks 1 and 4 without SCS (therapeutic effect). Box plots represent the median, 25th and 75th percentiles and minimum and maximum data points without outliers. All statistical significance was assessed with two-sided bootstrapping ($n = 10,000$): *$P < 0.05$, **$P < 0.01$, ***$P < 0.001$.

building on top of the newly acquired strength, SMA01 could stand up from a kneeling position when SCS was ON by week 4, and SMA03 could stand up from hinging on a desk by week 4 (Supplementary Videos 1–3), tasks that both participants were not able to do before the beginning of the study.

Effects of SCS on gait

To assess effects of SCS on functional tasks such as walking, we measured step height, step length, stride velocity and range of motion (ROM) at the hip and knee joints during overground walking using a 3D kinematic system (Vicon; Fig. 4a). Paralleling the results in strength, all participants improved in hip and knee ROM with SCS ON (Fig. 4d), suggesting a facilitatory effect on walking function. Additionally, SMA01 improved in stride velocity (Fig. 4b and Extended Data Fig. 5a), and SMA02 improved in step height, step length and stride velocity (Fig. 4b). Increases in ROM were paralleled by an increase in muscle activation (Extended Data Fig. 6b,c,f,g). To further demonstrate the immediacy of

the assistive effects, we asked SMA01, who could sustain longer walking periods, to exacerbate hip flexion during weight-supported treadmill walking. We then turned SCS ON and OFF and observed an immediate increase in step height when SCS was ON (Supplementary Video 4 and Extended Data Fig. 5g–i). Finally, we executed sham controls by delivering suboptimal SCS parameters and demonstrated that effects were SCS parameter dependent (Extended Data Fig. 5f).

We then examined the therapeutic effects of SCS by looking at how these variables changed over time. All participants significantly improved in all gait quality variables over time (stride velocity increased: SMA01 31%, from 91 cm s⁻¹, 95% CI: (89.3, 92.4) to 119.2 cm s⁻¹, 95% CI: (119, 120); SMA02 114%, from 22.6 cm s⁻¹, 95% CI: (22, 23.2) to 48.4 cm s⁻¹, 95% CI: (47, 50); SMA03 13%, from 54.2 cm s⁻¹, 95% CI: (52.8, 55.5) to 61.4 cm s⁻¹, 95% CI: (60.2, 62.6); Fig. 4c). Changes in gait quality were so prominent that SMA02, who, before the trial, could not flex his knee, completely changed his gait pattern by fully flexing the knee (+85% ROM at the knee, from 30.6°, 95% CI: (29.7, 31.5) to 56.6°,
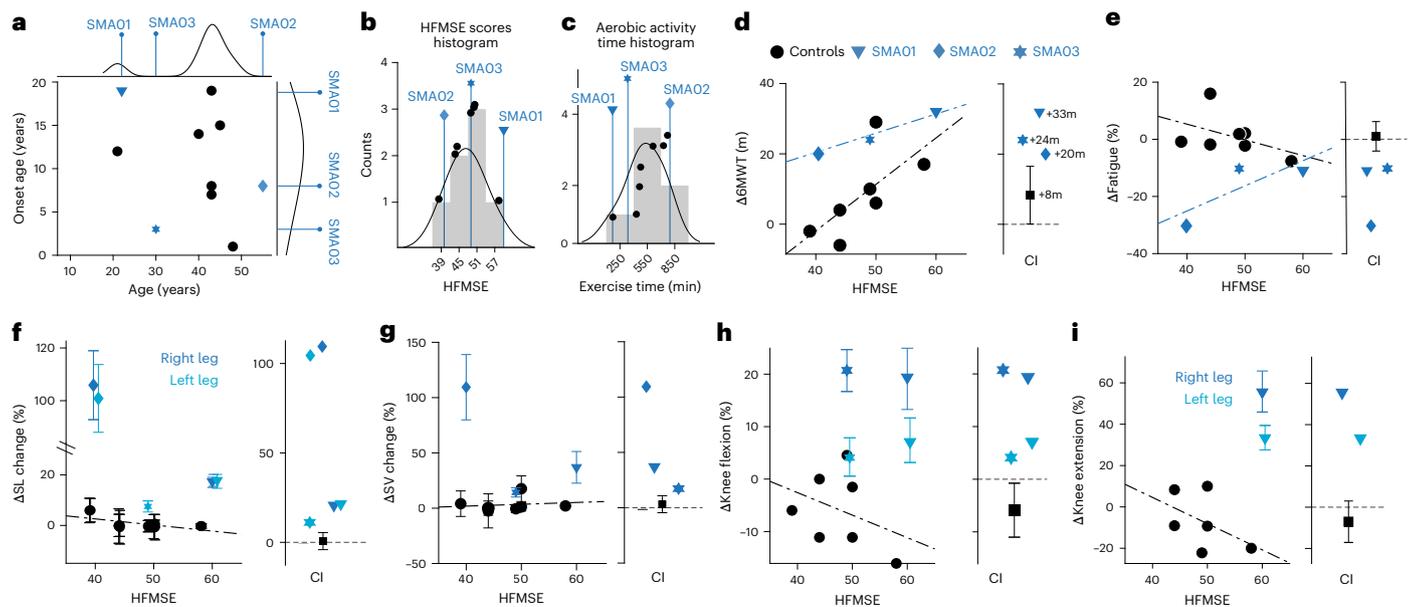
Fig. 5 | Comparison with aged-matched exercise-only control. Age-matched (>18 years old) exercise-only control group completed 3 months of aerobic and strength training[42]. **a**, Age versus disease onset age for the age-matched exercise-only control group (black) and the participants in our study (blue). **b**, Histogram of HFMSE scores for the control group (black); blue lines represent the HFMSE scores for each SCS participant. **c**, Histogram of aerobic exercise time for the control group (black); blue lines represent the exercise time for each of the SCS participants. **d**, Left, correlation between change in 6MWT score and HFMSE score for controls ($R^2 = 0.46$, slope = 1.32) and SCS participants ($R^2 = 0.98$, slope = 0.60). Right, mean and 95% CI of the mean change in 6MWT score across controls (black) and change for each SCS participant (blue). **e**, Left, linear regression analysis between the change in fatigue index during the 6MWT and the severity for both the control group ($R^2 = 0.2$) and the SCS participants

($R^2 = 0.7$). The fatigue index was computed as the percentage change in stride velocity between the sixth and first minute of the 6MWT. Right, mean and 95% CI of the mean change in fatigue across the controls (black) and changes for SCS participants (blue). **f**, Left, regression analysis between the change in stride length and severity for both controls ($R^2 = 0.39$) and SCS. Right, mean change and 95% CI in stride length across controls (black) and changes in SCS participants (blue). **g**, As in **f** for stride velocity ($R^2 = 0.02$). For the SCS participants, changes were computed during self-paced overground walking, comparing SCS OFF trials from weeks 1 and 4. **h**, Left, regression analysis between the change in strength during knee flexion for the controls ($R^2 = 0.13$). Improvements for SMA01 and SMA03 and their CIs are shown in blue. Right, mean and 95% CI of the knee flexion strength for the controls (black) and SCS participants (blue). **i**, As in **h** for knee extension ($R^2 = 0.23$). All CIs were computed with bootstrapping ($n = 10,000$).

95% CI: (54.9, 58.3) and +54% ROM at the hip, from 21.7°, 95% CI: (20.9, 22.5) to 33.5°, 95% CI: (31.9, 35); Fig. 4e and Supplementary Video 5). As expected, these improvements were paralleled by an increase in muscle activation (Extended Data Fig. 6d,e,h–j).

Comparison with an exercise-only control dataset
Although assistive effects are controlled against each participant's performance with SCS OFF, the changes that we observed over time (that is, therapeutic effects) could be confounded by the effects of physical exercise. Even though exercise is known to be ineffective in SMA[39,40], in the absence of internal controls we compared our results with data from a randomized clinical trial that directly tested the effects of exercise on motor function in the same patient population[41,42]. Specifically, we re-processed data from this trial for aged-matched controls ($n = 7$, Fig. 5; all participants $n = 11$ reported in Extended Data Fig. 7b–j). Control participants matched SMA01, SMA02 and SMA03 by both age and disease onset (Fig. 5a), by severity of the disease (HFMSE; Fig. 5b) and by total time-on-task for the exercises (Fig. 5c). Using this dataset, we compared endurance, fatigability, gait quality variables and muscle strength with our data. First, we found that all our participants improved by at least 20 m in the 6-minute walking test (6MWT) largely outperforming the control dataset[39] (SMA01: +32 m (+6.1%), SMA02: +20 m (+27.7%), SMA03: +24 m (+23.5%); Fig. 5d, Extended Data Fig. 7a and Supplementary Video 6). Changes in SMA01 were so large that he reported now being able to walk back from patient housing to the laboratory without fatigue. Control participants experienced a non-significant mean change in the 6MWT of +8 m. Additionally, controls showed a strong relationship between changes in the 6MWT and disease severity

(controls: slope = 1.32) with benefits appearing mostly for participants with lower severity. Instead, our participants showed a small dependency on severity (SCS participants: slope = 0.54) and large changes in the higher severity ranges. Second, we quantified fatigability as the difference in velocity between the first and last minute of the 6MWT[43]. All our participants decreased in fatigability, whereas no effect was observed for controls (Fig. 5e). Third, improvement in gait parameters such as stride length (Fig. 5f) and stride velocity (Fig. 5g) suggest that our participants were not simply improving walking distance but also changing gait patterns. Finally, changes in strength obtained with SCS were markedly higher than any other datapoint observed in the controls (Fig. 5h,i). Conclusions do not change when considering including minors (Extended Data Fig. 7) or outcomes at 6 months (Supplementary Information). In summary, our analysis suggests that our results cannot be explained only by the effects of physical exercise.

SCS improves spinal motoneuron function
Our leading hypothesis was that SCS improved motoneuron function in SMA by reversing the maladaptive changes that produce motoneuron low firing rates and hyperexcitability (Fig. 1a).

To test this hypothesis, we used high-density electromyography (HDEMG)[44] (Methods) during isometric maximal voluntary contractions and extracted single motoneuron discharges from knee muscles. Motoneurons in able-bodied individuals regularly reach peak firing rates above 100 Hz[45–47] at maximal contraction. Instead, the mean peak firing across our participants was 50.6 Hz (95% CI: (46.9, 54.3)), confirming a considerable reduction in maximal firing of human motoneurons in SMA. We then assessed the assistive effects of SCS on motor unit firing
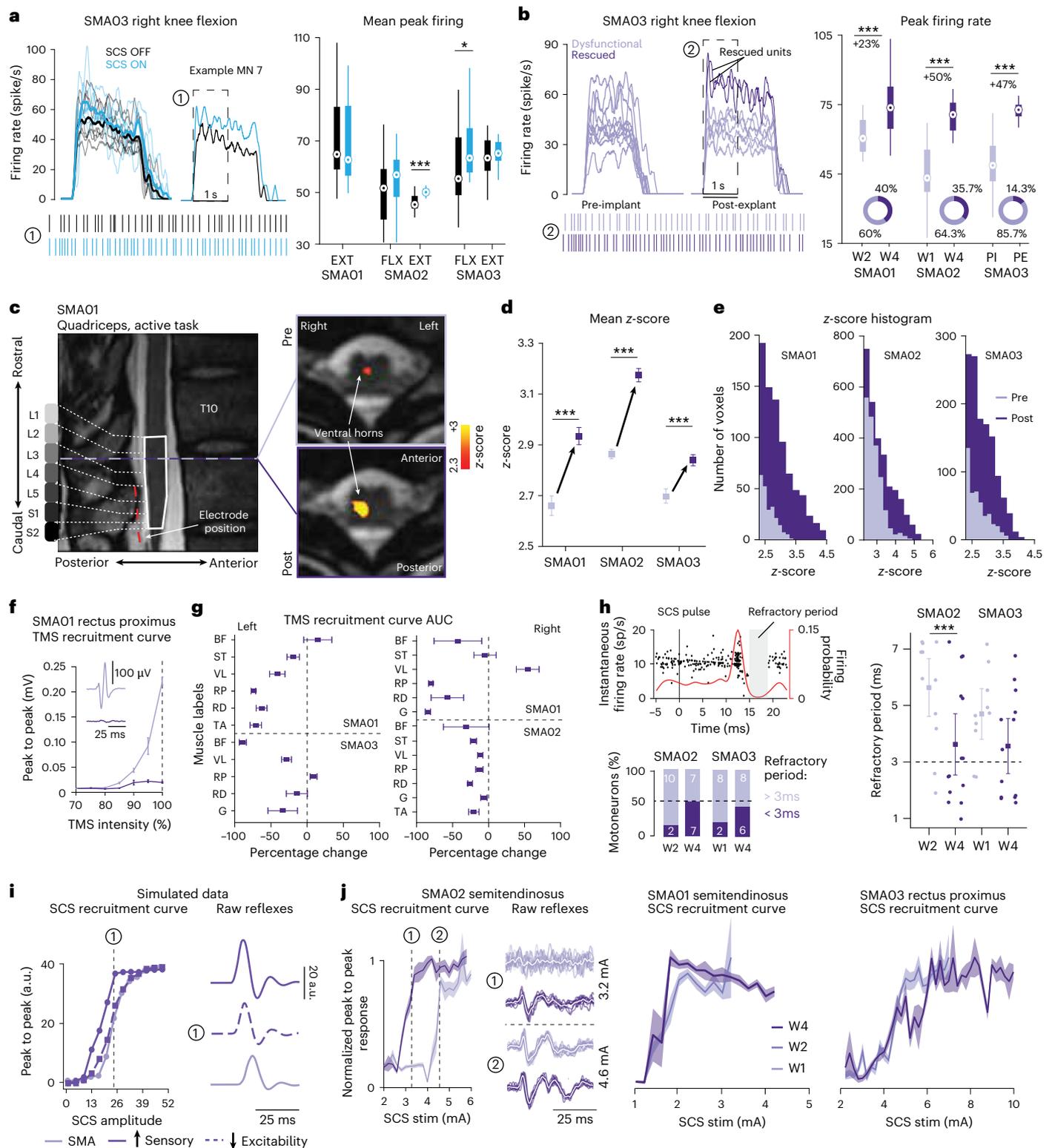
rates. We found that, when SCS was turned ON, some of the detected motor units increased their firing rates, which improved mean population firing in two of the five cases tested (SMA02 knee extension and SMA03 knee flexion; Fig. 6a). This correlates with the assistive changes in torques in experiments and simulations (Figs. 1g and 3a–c). We then looked at changes in motor unit firing over time with SCS OFF. Most of the post-explant unit firing dynamics was consistent with pre-implant values (Fig. 6b). However, post-explant, new motor units emerged that

appeared to have a markedly different behavior. These units showed higher peak firing rates (70.9 Hz, 95% CI: (67.4, 74.4)) at the onset of the force production. Then, mimicking motoneurons from able-bodied participants, the firing rate decayed over time rather than remaining flat[45–47] (Fig. 6b and Extended Data Fig. 8c,e,f). The distribution of peak firing rates for these units was markedly different from any other unit recorded pre-implant (Fig. 6b and Extended Data Fig. 8b); therefore, we labeled these units as 'rescued units'. Rescued units accounted for

Fig. 6 | Electrophysiological evidence of improvements in motoneuron function. a, Left, single motoneuron firing rates during an MVC in isometric condition with and without SCS. Raster plots show the spike times of two example motoneurons during the first second. Right, mean peak firing rates across all isometric trials for SCS ON and OFF. **b**, Left, traces of single-unit motoneuron firing rate for pre-implant (PI) versus post-explant (PE). Right, peak firing rate for all motoneurons identified in the first HDEMG session and the rescued motoneurons identified in the last sessions of HDEMG. Circles represent the percentage of rescued motor units recorded in the last HDEMG session. **c**, Spinal segments are reported in the T2 anatomical image of SMA01. Thresholded activity patterns of single pre and post scans (uncorrected, $Z > 2.3$, $P < 0.01$). **d**,**e**, Mean z-score (**d**) and histogram of z-scores (**e**) of the L1–S2 spinal segments thresholded activity pattern maps. **f**, Example of TMS recruitment curve and example mean waveforms at 100% intensity pre-implant versus post-explant. Error bars represent s.e.m. **g**, Percentage change in area under the curve of peak-to-peak TMS responses pre-implant versus post-explant across all intensities tested. **h**, Top left, example of a PSF. Bottom left, number of motoneurons with refractory periods shorter than 3 ms increased from early in the study (16.7% for SMA02 and 20% for SMA03) to the end of the study (43% for SMA02 and 50% for SMA03). Right, refractory period of single motoneurons. **i**, Biophysical model SCS recruitment curves for SMA-affected motoneuron pools. Light purple: 0% rescued motoneuron and sensory afferents. Solid purple: 50% rescued motoneurons and Ia-afferents. Dashed purple: 70% rescued motoneurons and 25% rescued sensory afferents. **j**, Mean and standard error of a normalized recruitment curve and raw waveforms. Box plots represent the median, 25th and 75th percentiles and minimum and maximum data points without outliers. All error bars indicate the mean 95% CI computed using bootstrapping ($n = 10,000$), otherwise specified. All statistical significance was assessed with two-sided bootstrapping ($n = 10,000$): *$P < 0.05$, **$P < 0.01$, ***$P < 0.001$. EXT, extension; FLX, flexion; MN, motoneuron.

a large proportion of detected units in all participants (40%, 36% and 14% for SMA01, SMA02 and SMA03, respectively) (Fig. 6b). Although we cannot discard other mechanisms, using our computer model we found that the improvements in torque could be explained just by the increase in motoneuron firing rates (Extended Data Fig. 1h,i).

We validated these results with an alternative measure of neural activity: blood-oxygenation-level-dependent (BOLD) signal in spinal cord fMRI. We designed fMRI sequences for the lumbosacral spinal cord while participants volitionally flexed and extended their knee (Fig. 6c–e and Extended Data Fig. 9). The fMRI images produced clear BOLD activation that matched the position of knee motoneurons (Fig. 6c). In all three participants, BOLD signal significantly increased (z-score) post-explant compared to pre-implant, indicating a sizable increase of neural activity (Fig. 6d,e).

Spinal cord neurostimulation changes motoneuron properties

In SMA, motoneurons have reduced synaptic inputs from Ia-afferents, which triggers an increase in excitability and low firing rates due to longer refractory periods (Fig. 1a). Therefore, if it is true that SCS reversed motoneuron dysfunction in SMA, then increases in motoneuron firing rates should be paralleled by decreases in motoneuron excitability, shorter refractory periods and an increase in synaptic inputs.

We first tested for motoneuron excitability using TMS. Indeed, in humans with SMA, the cortico-spinal tract is not affected by SMA[48]. Because SCS does not affect the cortico-spinal tract[34], this pathway constitutes an independent pathway to test motoneuron excitability using TMS. In simulations, a rescue of motoneuron function led to a decrease in peak-to-peak motor evoked potentials (MEPs) produced by single pulses of TMS (Extended Data Fig. 1j,k). We verified this by stimulating the leg area of the motor cortex with single TMS pulses. Similarly to simulations, after study, we observed a significant decrease in MEP peak-to-peak amplitudes in all three participants (Fig. 6f,g). At the same time, detected motor unit numbers did not change (Extended Data Fig. 8d), which suggests that the intrinsic excitability of spinal motoneurons decreased during the study, making it more difficult for TMS pulses to induce MEPs. When SCS was interrupted, MEPs increased back at 6 weeks post-explant (Extended Data Fig. 10a). To control for synaptic effects that could explain this result[49], we used our computer model to simulate the two alternatives—for example, motoneurons changed membrane properties versus a reduction in cortico-spinal synaptic strength. Our simulations show that TMS alone cannot resolve between these two alternatives (Extended Data Fig. 1j,k). However, a reduction in synaptic strength from cortico-spinal inputs cannot explain the increase in firing rates during isometric force tasks (Extended Data Fig. 1l,m), suggesting that changes in motoneuron membrane properties must have occurred.

Second, we measured the refractory period of motoneurons using the technique of the peri-stimulus frequencygram (PSF)[50,51]. Using this technique, we found that SCS pulses triggered action potentials followed by a total suppression of firing events due to each unit's unique refractory period (Fig. 6h); we measured the duration of this silent period to quantify the refractory period of each unit. At the beginning of the trial, the mean refractory period was approximately 5 ms (SMA02: 5.6 ms, 95% CI: (4.6, 6.65); SMA03: 4.7 ms, 95% CI: (3.8, 5.6); SMA01: we could not perform the experiment owing to time limitations), which is longer than what is considered normal in humans (2 ms[52]). However, at week 4, the mean refractory period for both SMA02 and SMA03 participants was 3.62 ms, 95% CI: (2.5, 4.7) for SMA02 and 3.6 ms, 95% CI: (2.6, 4.5) for SMA03. Notably, at the beginning of the study, SMA02 and SMA03 had only 16.7% (2/12) and 20% (2/10) of units with refractory periods shorter than 3 ms, respectively. At the end of the study, SMA02 and SMA03 had 43% (6/14) and 50% (9/18) of units with refractory periods shorter than 3 ms, respectively. Our results demonstrate that while administered, SCS reversed circuit dysfunctions, thereby decreasing motoneuron hyperexcitability and shortening motoneuron refractory periods (Fig. 1).

Finally, we evaluated changes in sensory-to-motoneuron synaptic strength. We analyzed the sensory reflexes elicited by single pulses of SCS in leg muscles in the first and last week of implant. We found that reflexes were either unchanged or increased in all three participants (Fig. 6j and Extended Data Fig. 10b). This is consistent with simulations that show that reflexes should either remain stable or increase in consequence of the balancing effects of increased excitatory inputs and decreased the motoneuron excitability (Fig. 6i).

In summary, after 4 weeks of SCS, we found (1) that a large proportion of motor units significantly increased their peak firing capacities; (2) a stronger BOLD fMRI signal in the spinal cord; (3) that TMS MEPs were substantially reduced in size; (4) that motor units had shorter refractory periods; and (5) that sensory synapses increased in strength. These combined findings constitute first proof that SCS reversed, at least while it is administered (2 h per day), the maladaptive changes that produced motoneuron dysfunction in humans with SMA.

Discussion

In this study, we demonstrated that electrical stimulation of the sensory afferents alleviated motor deficits in three humans with SMA through a combination of immediate assistive effects and therapeutic effects that appeared over time with SCS OFF. Importantly, we found evidence of improved spinal motoneuron function in an otherwise progressive neurodegenerative disease.

Although we cannot rule out that SCS induced additional changes at a broader circuit level, our electrophysiological and imaging data suggest that SCS altered motoneurons electrical properties, resulting in large and rapid changes in motor function. This is consistent with the hypothesis that people living with SMA have a set of surviving motoneurons, most of which have reduced firing capabilities that could be rescued by neurostimulation[53]. Notably, evidence of improved motoneuron function was consistent in all three participants: all showed rescued units, increased fMRI BOLD signal, decreased TMS, decreased

refractory periods and increased sensory inputs irrespective of their disease progression, age or SMN-inducing therapy status.

In addition to the immediate changes in strength when SCS was turned ON (assistive effects), we also observed unexpectedly large changes in strength and gait quality that persisted when SCS was OFF. Statistical analysis against data from a randomized clinical trial in adults with SMA exploring the effect of exercise suggests that our results cannot be explained by physical exercise only. This is not to say that exercise did not contribute in any way to the observed functional effects, but the addition of SCS led to large changes in behavior that could not be explained by existing data in humans.

To provide context for our functional gains, we obtained a minimum +20 m and a maximum +33 m change in 6MWT scores in 4 weeks. Recent reports on the efficacy of the clinically approved SMN-inducing drug nusinersen in ambulatory adults[54] show that people gain a minimum of 9 m and a maximum of 48 m in the 6MWT after 15 months. Therefore, we observed changes in the 6MWT that were similar to that reported in clinical studies of approved clinical treatments but obtained in only 4 weeks. We did not observe evidence of saturation or ceiling in improvements of both strength (Extended Data Fig. 4b–f) and kinematics (Extended Data Fig. 5b), as well as the number of rescued units (Fig. 6b), suggesting that a longer treatment may yield even larger effects. The different nature of SCS and existing therapies (SCS directly tackles the SMA circuit dysfunction, whereas current therapies induce SMN production) suggests that a synergistic intervention that combines both may lead to stronger recovery. Finally, follow-up at 6 weeks (and 6 months; Supplementary Information) shows that improvements may be lost if SCS is withdrawn, suggesting that SCS must be administered at least 2 h per day (as per our protocol) to retain gained function.

Although we did not observe any worsening of function, or other adverse events related to SCS, our study is limited by the short duration, which prevented us from assessing whether longer exposure to SCS may lead to detrimental motor effects that should be monitored for in future clinical studies. Notably, we think that future studies should consider enrolling only participants on SMN-inducing therapies to reduce risks for motoneurons. Finally, our data show that absolute improvement was stronger in our younger participant (SMA01), suggesting that early adoption is important, as disease progression could impact outcomes.

In summary, our results provide insights into the disease mechanisms of SMA that lead to circuit and motoneuron dysfunction in humans. Notably, we leveraged the identification of these mechanisms to design a clinically relevant intervention that manipulated the maladaptive processes induced by SMA, improving function at a cellular, circuit and behavioral level. Although SCS is being studied as an assistive neuroprosthetic tool to improve movement after spinal cord injury[29,55,56], stroke[30] and other neurodegenerative diseases[57–59], this is the first time, to our knowledge, that a neurostimulation therapy was not engineered to assist movement but, rather, to reverse degenerative circuit processes and effectively rescue motoneuron function in a human motoneuron disease.

Online content
Any methods, additional references, Nature Portfolio reporting summaries, source data, extended data, supplementary information, acknowledgements, peer review information; details of author contributions and competing interests; and statements of data and code availability are available at https://doi.org/10.1038/s41591-024-03484-8.

References

1. Yasuda, T., Nakata, Y. & Mochizuki, H. α-Synuclein and neuronal cell death. *Mol. Neurobiol.* **47**, 466–483 (2013).
2. Saxena, S. & Caroni, P. Selective neuronal vulnerability in neurodegenerative diseases: from stressor thresholds to degeneration. *Neuron* **71**, 35–48 (2011).
3. Blesa, J. & Przedborski, S. Parkinson's disease: animal models and dopaminergic cell vulnerability. *Front. Neuroanat.* **8**, 155 (2014).
4. Friedlander, R. M., Brown, R. H., Gagliardini, V., Wang, J. & Yuan, J. Inhibition of ICE slows ALS in mice. *Nature* **388**, 31–31 (1997).
5. Ona, V. O. et al. Inhibition of caspase-1 slows disease progression in a mouse model of Huntington's disease. *Nature* **399**, 263–267 (1999).
6. Li, M. et al. Functional role of caspase-1 and caspase-3 in an ALS transgenic mouse model. *Science* **288**, 335–339 (2000).
7. Friedlander, R. M. Apoptosis and caspases in neurodegenerative diseases. *N. Engl. J. Med.* **348**, 1365–1375 (2003).
8. Palop, J. J. & Mucke, L. Network abnormalities and interneuron dysfunction in Alzheimer disease. *Nat. Rev. Neurosci.* **17**, 777–792 (2016).
9. Palop, J. J. & Mucke, L. Amyloid-β–induced neuronal dysfunction in Alzheimer's disease: from synapses toward neural networks. *Nat. Neurosci.* **13**, 812–818 (2010).
10. Babiloni, C. et al. What electrophysiology tells us about Alzheimer's disease: a window into the synchronization and connectivity of brain neurons. *Neurobiol. Aging* **85**, 58–73 (2020).
11. Held, A. et al. Circuit dysfunction in *SOD1-ALS* model first detected in sensory feedback prior to motor neuron degeneration is alleviated by BMP signaling. *J. Neurosci.* **39**, 2347–2364 (2019).
12. Mentis, G. Z. et al. Early functional impairment of sensory-motor connectivity in a mouse model of spinal muscular atrophy. *Neuron* **69**, 453–467 (2011).
13. Mercuri, E. et al. Safety and efficacy of once-daily risdiplam in type 2 and non-ambulant type 3 spinal muscular atrophy (SUNFISH part 2): a phase 3, double-blind, randomised, placebo-controlled trial. *Lancet Neurol.* **21**, 42–52 (2022).
14. Tisdale, S. & Pellizzoni, L. Disease mechanisms and therapeutic approaches in spinal muscular atrophy. *J. Neurosci.* **35**, 8691–8700 (2015).
15. Lefebvre, S. et al. Identification and characterization of a spinal muscular atrophy-determining gene. *Cell* **80**, 155–165 (1995).
16. Arnold, W. D., Kassar, D. & Kissel, J. T. Spinal muscular atrophy: diagnosis and management in a new therapeutic era. *Muscle Nerve* **51**, 157–167 (2015).
17. Reilly, A., Chehade, L. & Kothary, R. Curing SMA: are we there yet? *Gene Ther.* **30**, 8–17 (2023).
18. Fletcher, E. V. et al. Reduced sensory synaptic excitation impairs motor neuron function via Kv2. 1 in spinal muscular atrophy. *Nat. Neurosci.* **20**, 905–916 (2017).
19. Alonso, L. M., Rue, M. C. & Marder, E. Gating of homeostatic regulation of intrinsic excitability produces cryptic long-term storage of prior perturbations. *Proc. Natl Acad. Sci. USA* **120**, e2222016120 (2023).
20. Simon, C. M. et al. Chronic pharmacological increase of neuronal activity improves sensory-motor dysfunction in spinal muscular atrophy mice. *J. Neurosci.* **41**, 376–389 (2021).
21. Blackburn, A. Z. et al. Spinal cord stimulation via percutaneous and open implantation: systematic review and meta-analysis examining complication rates. *World Neurosurg.* **154**, 132–143 (2021).
22. Capogrosso, M. et al. A computational model for epidural electrical stimulation of spinal sensorimotor circuits. *J. Neurosci.* **33**, 19326–19340 (2013).
23. Rattay, F., Minassian, K. & Dimitrijevic, M. R. Epidural electrical stimulation of posterior structures of the human lumbosacral cord: 2. quantitative analysis by computer modeling. *Spinal Cord* **38**, 473–489 (2000).
24. McIntyre, C. C. & Grill, W. M. Extracellular stimulation of central neurons: influence of stimulus waveform and frequency on neuronal output. *J. Neurophysiol.* **88**, 1592–1604 (2002).

25. Formento, E. et al. Electrical spinal cord stimulation must preserve proprioception to enable locomotion in humans with spinal cord injury. *Nat. Neurosci.* **21**, 1728–1741 (2018).

26. Moraud, E. M. et al. Mechanisms underlying the neuromodulation of spinal circuits for correcting gait and balance deficits after spinal cord injury. *Neuron* **89**, 814–828 (2016).

27. Balaguer, J.-M. et al. Supraspinal control of motoneurons after paralysis enabled by spinal cord stimulation. Preprint at *medRxiv* https://doi.org/10.1101/2023.11.29.23298779 (2023).

28. Booth, V., Rinzel, J. & Kiehn, O. Compartmental model of vertebrate motoneurons for Ca^{2+}-dependent spiking and plateau potentials under pharmacological treatment. *J. Neurophysiol.* **78**, 3371–3385 (1997).

29. Wagner, F. B. et al. Targeted neurotechnology restores walking in humans with spinal cord injury. *Nature* **563**, 65 (2018).

30. Powell, M. P. et al. Epidural stimulation of the cervical spinal cord for post-stroke upper-limb paresis. *Nat. Med.* **29**, 689–699 (2023).

31. Kinany, N. et al. Towards reliable spinal cord fMRI: assessment of common imaging protocols. *Neuroimage* **250**, 118964 (2022).

32. Capogrosso, M. et al. Configuration of electrical spinal cord stimulation through real-time processing of gait kinematics. *Nat. Protoc.* **13**, 2031–2061 (2018).

33. Rowald, A. et al. Activity-dependent spinal cord neuromodulation rapidly restores trunk and leg motor functions after complete paralysis. *Nat. Med.* **28**, 260–271 (2022).

34. Greiner, N. et al. Recruitment of upper-limb motoneurons with epidural electrical stimulation of the primate cervical spinal cord. *Nat. Commun.* **12**, 435 (2021).

35. Sharpe, A. N. & Jackson, A. Upper-limb muscle responses to epidural, subdural and intraspinal stimulation of the cervical spinal cord. *J. Neural Eng.* **11**, 016005 (2014).

36. Hofstoetter, U. S. et al. Periodic modulation of repetitively elicited monosynaptic reflexes of the human lumbosacral spinal cord. *J. Neurophysiol.* **114**, 400–410 (2015).

37. Hultborn, H. et al. On the mechanism of the post-activation depression of the H-reflex in human subjects. *Exp. Brain Res.* **108**, 450–462 (1996).

38. Šarabon, N., Kozinc, Ž. & Perman, M. Establishing reference values for isometric knee extension and flexion strength. *Front. Physiol.* **12**, 767941 (2021).

39. Bartels, B., Montes, J., van der Pol, W. L. & de Groot, J. F. Physical exercise training for type 3 spinal muscular atrophy. *Cochrane Database Syst. Rev.* **3**, CD012120 (2019).

40. Mercuri, E., Sumner, C. J., Muntoni, F., Darras, B. T. & Finkel, R. S. Spinal muscular atrophy. *Nat. Rev. Dis. Prim.* **8**, 52 (2022).

41. Montes, J. et al. A randomized, controlled clinical trial of exercise in patients with spinal muscular atrophy: methods and baseline characteristics. *J. Neuromuscul. Dis.* **1**, 151–161 (2014).

42. Montes, J. et al. Single-blind, randomized, controlled clinical trial of exercise in ambulatory spinal muscular atrophy: why are the results negative? *J. Neuromuscul. Dis.* **2**, 463–470 (2015).

43. Montes, J. et al. Six-Minute Walk Test demonstrates motor fatigue in spinal muscular atrophy. *Neurology* **74**, 833–838 (2010).

44. Farina, D. et al. Estimation of single motor unit conduction velocity from surface electromyogram signals detected with linear electrode arrays. *Med. Biol. Eng. Comput.* **39**, 225–236 (2001).

45. Del Vecchio, A. et al. You are as fast as your motor neurons: speed of recruitment and maximal discharge of motor neurons determine the maximal rate of force development in humans. *J. Physiol.* **597**, 2445–2456 (2019).

46. Van Cutsem, M., Duchateau, J. & Hainaut, K. Changes in single motor unit behaviour contribute to the increase in contraction speed after dynamic training in humans. *J. Physiol.* **513**, 295–305 (1998).

47. Del Vecchio, A., Falla, D., Felici, F. & Farina, D. The relative strength of common synaptic input to motor neurons is not a determinant of the maximal rate of force development in humans. *J. Appl. Physiol.* **127**, 205–214 (2019).

48. Norton, J. A., Roy, F. D. & Mahood, J. K. Preservation of motor evoked potentials under anesthesia in children with spinal muscular atrophy type II undergoing spinal deformity surgery. *J. Clin. Neurophysiol.* **30**, 382–385 (2013).

49. Jiang, Y.-Q., Zaaimi, B. & Martin, J. H. Competition with primary sensory afferents drives remodeling of corticospinal axons in mature spinal motor circuits. *J. Neurosci.* **36**, 193–203 (2016).

50. Türker, K. S. & Cheng, H. B. Motor-unit firing frequency can be used for the estimation of synaptic potentials in human motoneurones. *J. Neurosci. Methods* **53**, 225–234 (1994).

51. Metz, K. et al. Post-activation depression from primary afferent depolarization (PAD) produces extensor H-reflex suppression following flexor afferent conditioning. *J. Physiol.* **601**, 1925–1956 (2023).

52. Borg, J. Refractory period of single motor nerve fibres in man. *J. Neurol. Neurosurg. Psychiatry* **47**, 344–348 (1984).

53. Simon, C. M. et al. Dysfunction of proprioceptive sensory synapses is a pathogenic event and therapeutic target in mice and humans with spinal muscular atrophy. Preprint at *medRxiv* https://doi.org/10.1101/2024.06.03.24308132 (2024).

54. Arslan, D. et al. Nusinersen for adults with spinal muscular atrophy. *Neurol. Sci.* **44**, 2393–2400 (2023).

55. Angeli, C. A. et al. Recovery of over-ground walking after chronic motor complete spinal cord injury. *N. Engl. J. Med.* **379**, 1244–1250 (2018).

56. Gill, M. L. et al. Neuromodulation of lumbosacral spinal networks enables independent stepping after complete paraplegia. *Nat. Med.* **24**, 1677–1682 (2018).

57. Squair, J. W. et al. Implanted system for orthostatic hypotension in multiple-system atrophy. *N. Engl. J. Med.* **386**, 1339–1344 (2022).

58. Milekovic, T. et al. A spinal cord neuroprosthesis for locomotor deficits due to Parkinson's disease. *Nat. Med.* **29**, 2854–2865 (2023).

59. Hofstoetter, U. S., Freundl, B., Lackner, P. & Binder, H. Transcutaneous spinal cord stimulation enhances walking performance and reduces spasticity in individuals with multiple sclerosis. *Brain Sci.* **11**, 472 (2021).

[1]Department of Neurological Surgery, University of Pittsburgh, Pittsburgh, PA, USA. [2]Rehab Neural Engineering Labs, University of Pittsburgh, Pittsburgh, PA, USA. [3]Department of Bioengineering, University of Pittsburgh, Pittsburgh, PA, USA. [4]Department of Mechanical engineering, Carnegie Mellon University, Pittsburgh, PA, USA. [5]NeuroMechatronics Lab, Carnegie Mellon University, Pittsburgh, PA, USA. [6]Department of Neurology, University of Pittsburgh, Pittsburgh, PA, USA. [7]Department of Physical Medicine and Rehabilitation, University of Pittsburgh, Pittsburgh, PA, USA. [8]Department of

Biomedical Engineering, Carnegie Mellon University, Pittsburgh, PA, USA. ⁹The Neuroscience Institute, Carnegie Mellon University, Pittsburgh, PA, USA. ¹⁰Department of Neurology and Clinical Neurosciences, Stanford University, Palo Alto, CA, USA. ¹¹Genentech Roche, San Francisco, CA, USA. ¹²Department of Rehabilitation and Regenerative Medicine, Columbia University, New York, NY, USA. ¹³Spinal Muscular Atrophy Foundation New York, New York, NY, USA. ¹⁴Center for Motor Neuron Biology and Disease, Columbia University, New York, NY, USA. ¹⁵Department of Neurology, Columbia University, New York, NY, USA. ¹⁶Department of Pathology and Cell Biology, Columbia University, New York, NY, USA. ¹⁷Clinical and Translational Science Institute (CTSI), University of Pittsburgh, Pittsburgh, PA, USA. ¹⁸These authors contributed equally: Genís Prat-Ortega, Scott Ensel, Serena Donadio. ¹⁹These authors jointly supervised this work: Elivra Pirondini, Robert M. Friedlander and Marco Capogrosso. ✉e-mail: elvirap@pitt.edu; friedlanderr@upmc.edu; mcapo@pitt.edu

Methods

More information about the clinical trial, surgical procedures, EMG acquisition and analysis, biophysical model, statistical methods, MRI and fMRI pre-processing and analysis and SCS stimulators can be found in the Supplementary Information.

Trial and participant information

All experimental protocols were approved by the University of Pittsburgh IRB (protocol STUDY21080158) under an abbreviated investigational device exemption. The study protocol is publicly available on ClinicalTrials.gov (NCT05430113). Three male individuals actively took part in the study, participating in every experiment. When participants had specific limitations, we adjusted certain procedures accordingly, clearly indicating such cases. Before their involvement, participants underwent an informed consent process, in accordance with the procedure approved by the IRB. Participants received compensation for each day of the trial as well as for their travel and lodging expenses during the study period.

Inclusion criteria

Individuals aged 16–65 years, diagnosed with 5q-autosomal recessive SMA confirmed through genetic testing for a deletion in the *SMN1* gene (5q12.2-q13.3), were eligible for participation if the disease manifested after 18 months of age and after the acquisition of ambulation (type 3 or type 4 SMA). All our participants were male; thus, we could not perform sex analysis. All participants were required to be capable of standing independently for at least 3 s and have a pre-study Revised Hammersmith Scale (RHS) score equal to or lower than 65. Before enrollment, individuals underwent a medical evaluation for screening. Those with severe comorbidities, implanted medical devices preventing MRI or claustrophobia or those who were pregnant or breastfeeding were excluded from the study. Throughout the study period, participants were not allowed to take any anti-spasticity, anti-epileptic or anti-coagulation medications.

Study design and data reported

The objective of this exploratory clinical trial is to obtain preliminary evidence of safety and efficacy of SCS as a potential treatment to enhance motor function in individuals diagnosed with type 3 SMA. The study is structured as a single-center, open-label, non-randomized trial. We expect to enroll up to six individuals exhibiting quantifiable motor deficits in the legs but capable of independent standing. Given the pilot nature of the study, SCS leads are implanted for a maximum of 29 days to minimize safety risks, after which the electrodes are removed. The primary and secondary outcomes are designed to primarily assess safety and obtain initial clinical and scientific evidence regarding both the assistive and therapeutic effects of SCS (Supplementary Information).

After screening and establishment of pre-study baselines, participants undergo implantation of percutaneous, bilateral, linear spinal leads near the lumbar spinal cord. Scientific sessions are conducted five times per week, lasting 4 h each, totaling 19 sessions, starting from day 4 post-implant. Tasks and measurements in the initial 2 weeks focus on identifying optimal SCS configurations, which are then maintained for the remaining sessions. The primary outcomes aim to assess safety by monitoring adverse events related to SCS use. Participants rate the 'discomfort/pain' on a scale of 1 to 10 for each SCS configuration to ensure that SCS intensities required for motor function improvement remain within a range of non-painful sensations. Additionally, the primary outcomes evaluate the effects of SCS on specific motor control variables. We quantify assistive and therapeutic improvements in strength by measuring isometric torque with and without SCS regularly during the trial. We rate motor deficits by assessing the HFMSE and the 6MWT pre-implant and post-explant. We then evaluate function by measuring 3D kinematics during overground walking with and without SCS.

Secondary outcomes aim to acquire scientific evidence of mechanisms that may contribute to improved motor performance. A battery of imaging and electrophysiology tests assesses early signs of neural plasticity in the central nervous system associated with measured effects on motor control. A comprehensive description of primary and secondary outcomes can be found on ClinicalTrials.gov (NCT05430113). This paper reports results from the first three participants.

Participant information

Here we report the results from the first three individuals participating in our trial. All participants were diagnosed with SMA type 3 and were able to stand and walk (with the assistance of walking aids for SMA02 and SMA03). SMA01 (Hispanic male, 22 years old) had mild motor deficits with an HFMSE at enrollment of 60/66 points. He was not under any treatment during the duration of the study. SMA02 (white male, 55 years old) had the most severe motor deficit, with HFMSE at enrollment of 40/66 points. During the study, he was under nusinersen. For safety reasons, he performed all the overground walking sessions with the use of the unweighing system (Biodex, NxStem), except the 6MWT. SMA03 (white male, 30 years old) had moderate motor deficit, with HFMSE at enrollment of 49/66 points. During the study, he was under nusinersen. A previous surgery on his right hip affected his gait. Thus, all kinematic analysis was focused on his left leg.

Safety

We meticulously documented all adverse events and promptly reported them to both the data safety and monitoring board (DSMB) and the IRB for a thorough evaluation of their potential association with the delivery of electrical stimulation to the spinal cord. Fortunately, all participants successfully completed the protocol without encountering any serious adverse events. The only non-serious adverse events were falls during the execution of exercises or during breaks between exercises that did not result in injuries (each participant fell once). None of these falls sustained any injuries. Risk mitigation strategies included the use of straps and harnesses and the continuous presence of a physical therapist during exercises. This precautionary approach is crucial to ensure the safety of participants and underscores the importance of implementing robust measures to minimize the risk of falls during the course of the study.

Single-joint isometric torque

Torque measurement. The torques produced during MVC were measured for hip flexion/extension and knee flexion/extension using a robotic torque dynamometer (CSMi, HUMAC NORM). We tested the maximum torque produced by participants at the knee and hip extension/flexion pre-implant, post-explant and during the 4 weeks of SCS (knee extension/flexion two times per week, hip extension/flexion at least twice). Measurements below 4 Nm were not reliable due to the biomechanical noise of our system. This was particularly important for SMA02 where we could measure torque only in his right hip. Instead, for SMA01, we could measure all joints and, for SMA03, all joints except knee extension (Fig. 3 and Extended Data Figs. 3 and 4). See Supplementary Information for more information.

Analysis of the assistive effect in maximum torque. In every session, we measured the torque produced without SCS and repeated the same measurements with SCS. We computed the percentage of increase with SCS and the CIs with bootstrapping ($n = 10,000$) (Fig. 3d).

Analysis of the therapeutic effect in maximum torque. We computed the percentage increase in torque without SCS pre-implant versus post-explant (4 or 5 days after explant) and used bootstrapping ($n = 10,000$) to compute the CI and level of significance (Fig. 3d–f and Extended Data Fig. 3a).

SCS sham experiments. To rule out placebo effect in the assistive improvements in strength, we compared the MVC produced by the participants with the optimal SCS parameters and random parameters. The random parameters were chosen to not target the specific muscles involved in the joint movement being tested or by changing stimulation frequency while being sensory indistinguishable for our participants. To do so, we first performed six repetitions without SCS, and then we performed the six repetitions with optimal and sham parameters in randomly ordered sets of three repetitions.

Kinematic curves, gait variables and EMG envelope

Once per week during the study, participants were instructed to walk back and forth at a comfortable speed in the gait laboratory. We combined trials with and without SCS, and we took breaks between laps to prevent fatigue. We placed 16 retroreflective markers on the surface of the skin and used the Vicon Motion Capture system with 12 infrared cameras (100-Hz frame rate) and three optical cameras (60-Hz frame rate) to track the movement of the participants. We recorded the EMG activity of seven different muscles in each leg (Supplementary Information).

Joint angle motions were computed using Nexus biomechanical software (Vicon, Nexus 2.12.1). We developed custom software in MATLAB R2023a to detect gait events (foot strike/foot off). We segmented the data between two consecutives foot strikes of the same leg and defined this as one gait cycle. We high-pass filtered (first-order Butterworth high-pass filter, cutoff frequency of 0.01 Hz) and segmented the data to remove offsets between sessions due to slight changes in the placement of the markers. Finally, we resampled each gait cycle to have 101 samples.

We computed the ROM of each joint angle across the gait cycle and analyzed the percentage change for the assistive effects (SCS ON versus OFF, week 1) and therapeutic effects (week 1 versus week 4, SCS OFF) (Fig. 4d,e). Gait variables (step length, step height and stride velocity) were computed based on the 3D trajectory of the heel markers. Specifically, step length was determined as the distance covered in the direction of motion between two consecutives foot strikes of different legs; step height was measured as the maximum height during each step; and stride velocity was calculated as the ratio of stride length (distance between consecutive foot strikes of the same leg) to stride duration. For SMA01 and SMA02, we computed these parameters for both legs. However, for SMA03, we used the data from only the left leg because the gait of his right leg was affected by a surgery previous to this study. To evaluate the assistive effects, we pooled together all data from the sessions with stimulation, and we normalized by the median of each session without stimulation. For the long-term effects, we normalized the gait variables using the median values from the pre-implant or from week 1 if pre-implant data were unavailable (Fig. 4b,c).

Single motoneuron firing rate analysis

Motoneuron decomposition. We recorded HDEMG from knee extensors (that is, rectus femoris) and flexors (that is, biceps femoris) while the participants performed two sets of three MVC. An 8 × 8 channel flexible high-density surface electromyography (HDsEMG) grid electrode with 8.75-mm distance between electrodes was placed over the rectus femoris and biceps femoris muscles, respectively. Conductive gel was used to reduce the skin–electrode impedance. At the end of each experimental session, the edges of the grid were traced on the participants' skin using a skin marker to ensure consistent grid placement throughout the different phases of the clinical study (that is, pre-implant; *i*th week after the implant; post-explant). EMG recordings were acquired in monopolar configuration, with the reference electrode placed over the patella, using a TMSi Saga 64+ high-density amplifier at a sampling rate of 4 kHz. We then decompose the HDsEMG recordings into the spike train of individual motoneurons using DEMUSE tool software, which exploits the convolution kernel compensation method[60] (Extended

Data Fig. 8a). The results of this automatic decomposition were manually edited following the standard procedure previously described[61,62]. Only motoneurons with pulse-to-noise ratio ≥ 30 dB[63] were selected for further analysis.

Rescued motoneuron identification. To assess changes in the motoneuron firing properties during the clinical study, we compared the peak firing rate of motoneurons without SCS between the first and last sessions where we recorded HDsEMG (week 2 versus week 4 in SMA01, week 1 versus week 4 for SMA02 and pre-implant versus post-explant in SMA03). We created a unique set of motoneurons per experimental session; motoneurons were tracked across the two sets of MVC using the motor unit filter transfer method[64]. However, it was not possible to track motoneurons across different experimental sessions. We calculated the motoneuron firing rate in a 100-ms overlapping window and subsequently smoothed with a 100-ms moving average window to obtain the smoothed discharge rate. A post-explant motoneuron was considered functionally rescued when its mean peak firing was above the 99.73% CI of the mean peak firing rate among the pre-study motoneurons (Extended Data Fig. 8b). We computed this CI using bootstrapping ($n = 10,000$). To test the hypothesis that functionally rescued motoneurons have a higher firing rate, we performed a two-sided significance test using bootstrap ($n = 10,000$).

Comparison SCS ON versus SCS OFF. To evaluate changes in motoneuron firing rate mediated by SCS, we tracked the same motoneurons in trials with and without SCS using the motoneuron filter transfer method[64]. We used the motoneurons that we could track in both conditions to compare the mean peak firing rate with and without SCS. To test the hypothesis that motoneurons have higher firing rate in SCS ON versus OFF conditions, we performed a two-sided significance test using bootstrapping ($n = 10,000$).

Analysis of the motoneuron firing dynamics. To assess differences in firing rate between rescued and dysfunctional motoneurons at the start and end of the MVC, we analyzed post-explant motoneurons for each participant (Extended Data Fig. 8e,f). We pooled together all motoneurons from all repetitions and movements (flexion and extension). To mark the start and end of the contraction, we used a MATLAB algorithm that identifies the first and last significant peaks within the active window. For both the start and end of the contraction, we extracted a 150-ms segment, centered in the identified peak. Within these segments, we calculated the mean firing rate. Finally, we computed the percentage change in mean firing rate between dysfunctional and rescued motor units at both the start and end of the MVC. We computed the 95% CI using bootstrapping ($n = 10,000$). We tested significance using a two-sided test with bootstrapping.

Refractory period measurement

To assess changes in the motoneuron membrane properties, we measured their refractory period by estimating the firing probability based on the PSF[50,51]. The PSF represents the instantaneous discharge rate against the time of the stimulus for each motor unit. When suprathreshold SCS stimuli are delivered, a period of silence follows the motoneurons' membrane depolarization (that is, refractory period) (Fig. 6h). To measure the duration of the silent period, we estimated the probability density function (MATLAB's inbuilt function 'kde' (MathWorks, MATLAB (R2023b))) for the instantaneous motoneuron firings, which correlates to the likelihood of finding a motoneuron spike in a specific time after the stimulus. Finally, to identify the start and end of the silent period, we used a thresholding method. We detected the beginning and the end of the silent period when the firing probability was lower and higher than 1%, respectively. Finally, we visually inspected silent periods to exclude those that erroneously included the SCS pulses or others in which the algorithm detected silent periods

in which there was actually firing. We used a two-sided significance test using bootstrapping ($n = 10,000$) to test differences in refractory period during the first and last HDEMG sessions.

TMS

Magnetic stimulation was applied to M1 by a Magstim 200 through a figure-of-eight coil (70-mm loop diameter, D70) with single, monophasic pulses (Magstim Company). Measurements were taken using the 10–20 system to identify scalp locations corresponding to the vertex (Cz) and approximately 1 cm lateral of the vertex line, in line with the tragus of the ear and contralateral to the target muscle. The optimal scalp site was determined by stimulating this location and moving the coil in increments anterior-posterior/medial-lateral directions following a 5 × 5-cm grid with 1-cm spacings. The coil was also rotated to identify the optimal angle relative to the mid-sagittal plane. The location and angle that produced stable MEPs at the near threshold stimulator outputs was set as the optimal location and recorded by a frameless, stereotaxis neuronavigation system (Rogue Research, Brainsight). Coil location and orientation were adjusted by the experimenters throughout the duration of each experiment using feedback provided by the neuronavigation system. At the optimal targets, stimulation was applied for five or 10 pulses with an inter-stimulus interval of at least 5 s. Stimulation intensity was stepped from 60% of stimulator output to 100% at increments of 5%. This test was performed pre-implant, third week of trial, post-explant and 6-weeks follow-up. SMA01 could not perform the follow-up TMS session.

Recruitment curves

To evaluate the specificity of SCS in recruiting individual motor pools, recruitment curves were performed on representative contacts of the lead, and optimal configurations were found throughout testing. We used a wireless EMG system (Delsys, Trigno) to record compound muscle action potentials (CMAPs) elicited by SCS pulses. SCS was delivered at 1–2 Hz on one electrode at a time with gradually increasing current amplitude while simultaneously recording CMAPs from all muscles. The peak-to-peak amplitude of the SCS-induced CMAPs were measured, one for each stimulus amplitude, and normalized to the maximum amplitude recorded on that muscle across all measured trials.

Functional imaging data

Active task. During each scan session, participants completed three 6-min runs composed of 16-s blocks of active knee extension where the knee is extended and relaxed at a rate of 0.5 Hz. One run consisted of nine active extension blocks. The aim was to target the quadriceps and hamstring muscles. A custom software implemented in PsychToolbox version 3.0.17 allowed instructions and repetitions to synchronize with the MRI acquisitions. Instructions were displayed on a screen (fixation cross '+' during rest blocks and text indicating activity blocks), and auditory cues were used to signal changing blocks. Only the participant's right leg was tested. See Extended Data Fig. 9 and Supplementary Methods for details on fMRI data, 'Processing and analysis'.

Clinical evaluations

HFMSE. The HFMSE was developed for patients with SMA who are ambulatory. The HFMSE consists of 33 items that are scored 0, 1 or 2. A score of 2 is assigned to participants who achieve the motor task without any compensatory strategies. Attempted movements or items achieved with compensation are scored a 1. A score of 0 is assigned to those unable to perform the task. The same licensed therapist administered and scored HFMSE tests pre-implant and post-explant.

6MWT

The 6MWT is a submaximal exercise test of endurance and aerobic capacity. Participants are instructed to 'walk as far as possible for 6 minutes'. The distance walked over the course of 6 min is measured in a structured environment. The 6MWT is routinely implemented to assess changes in basic mobility in patients with SMA. We compute the fatigability index as the percentage change in velocity between the first and last lap. The same licensed therapist administered and scored the 6MWT pre-implant and post-explant.

Reporting summary

Further information on research design is available in the Nature Portfolio Reporting Summary linked to this article.

References

60. Holobar, A. & Zazula, D. Multichannel blind source separation using convolution kernel compensation. *IEEE Trans. Signal Process.* **55**, 4487–4496 (2007).
61. Del Vecchio, A. et al. Tutorial: analysis of motor unit discharge characteristics from high-density surface EMG signals. *J. Electromyogr. Kinesiol.* **53**, 102426 (2020).
62. Hug, F. et al. Analysis of motor unit spike trains estimated from high-density surface electromyography is highly reliable across operators. *J. Electromyogr. Kinesiol.* **58**, 102548 (2021).
63. Holobar, A., Minetto, M. A. & Farina, D. Accurate identification of motor unit discharge patterns from high-density surface EMG and validation with a novel signal-based performance metric. *J. Neural Eng.* **11**, 016008 (2014).
64. Frančič, A. & Holobar, A. On the reuse of motor unit filters in high density surface electromyograms with different signal-to-noise ratios. In *8th European Medical and Biological Engineering Conference* (eds Jarm, T. et al.) 923–931 (Springer International, 2021).

Author contributions

M.C., R.M.F. and M.J.L.E. conceived the study. G.P.O., S.E. and S.D. performed and designed all experiments and analyzed the data. L.B. and N.V. performed single motoneuron experiments. G.P.O., S.E., S.D. and L.B. created figures. L.B., P.Y., N.V. and D.W. analyzed single motoneuron data. A.B. performed all clinical evaluations, under the

Extended Data Fig. 1 | See next page for caption.

Extended Data Fig. 1 | Biophysical model. a-b Rheobase for WT and SMA motoneuron biophysical models. To compute the rheobase we slowly increased the input current injected to the motoneuron's soma (**a**) until a spike was triggered (**b**). The black and purple lines indicated the rheobase, the smallest amplitude that triggers an action potential. The SMA motoneuron biophysical model reproduces the active hyperexcitability characterized by reduced rheobase. **c**, Example of 2 second isometric force produced by a SMA-affected motoneuron pool simulated with the biophysical model. From bottom to top: Raster plot of 11 Ia-afferent fibers recruited by SCS at 40 Hz. Note that spikes are completely synchronized because they are triggered by SCS pulses. Supraspinal neurons with natural firing rate (Poisson neurons); for visualization propose, we only show 11 neurons but the supraspinal population has 200 neurons. Motoneuron pool firing rate with 30% of motoneuron loss and 50% SMA-affected motoneurons. Simulated force produced by the motoneuron pool normalized by the maximum force produced by an intact motoneuron pool. **d**, SMA-affected motoneuron pool firing rate for different simulated percentage of motoneuron loss and SMA-affected motoneurons. **e**, Simulated force for different percentages of motoneuron loss and SMA-affected motoneurons. **f**, Motoneuron pool firing rate as a function of the supraspinal firing rate with SCS ON and OFF. The biophysical model predicted that the effect of SCS should be more prominent on low than high supraspinal inputs indicating that if all motoneurons are recruited at their maximum firing rate, there should be no effect of SCS. Thus, the effect of SCS at maximum voluntary contraction will depend on the participants' ability to recruit the resources of their motoneuron pool. SCS could give access to motoneurons that are not recruited or recruited with a submaximal firing rate. **g**, Simulated force with a low supraspinal input (5 Hz) and very high supraspinal input (50 Hz). **h**, Firing rate for a SMA-affected pool with all SMA-affected motoneurons and 40% rescued which is the percentage of

rescued motoneurons for SMA01 Right Knee Extension. **i**, Predicted forces by the biophysical model given the percentage of motoneurons rescued in SMA01 Right Knee Extension and SMA03 Right Knee Flexion. First, we simulated the torque produced with a SMA-affected pool with 70 motoneurons all affected by SMA (light purple). In purple we simulated the torque rescuing the same percentage that we found experimentally: 40% for SMA01 Right Knee Extension and 25% SMA03 Right Knee Flexion. Finally, we used a bootstrap method to generate multiple predictions of the percentage of rescued units per participant, to estimate a maximum possible upper limit that could occur by random variations in the data (95th percentile). Using this method we found that the maximum percentages of rescued motoneuron consistent with our data were 80% and 50% for SMA01 Right Knee Extension and SMA03 Right Knee Flexion respectively. We simulated the torques with these upper limits (dark purple) and we found that the experimental values (dash black line) fell below the upper boundary. For SMA01 our biophysical model predicted an increase of 24% and up to 69% which is consistent with the experimental increase in right knee extension +55%. For SMA03 our model predicted an increase in torque of 15% and up to 42% which is remarkably consistent with the +21% increase that we found in right knee flexion. All simulated torques are normalized by the torque produced by a SMA-affected motoneuron pool with 70 SMA-motoneurons. **j**, Simulated peak to peak of the TMS MEP for two hypotheses: reversion of the maladaptive changes produced by SMA (SMA rescued) and reduction of the supraspinal synaptic weight. **k**, Examples of simulated MEP. Both hypotheses are consistent with experimental findings of smaller MEP. **l,m**, Simulated firing rates as a function of the supraspinal inputs (**l**) and simulated torque (**m**) for the two hypotheses. Only the hypothesis of rescued motoneurons is consistent with the experimental findings of higher firing rates and torques.
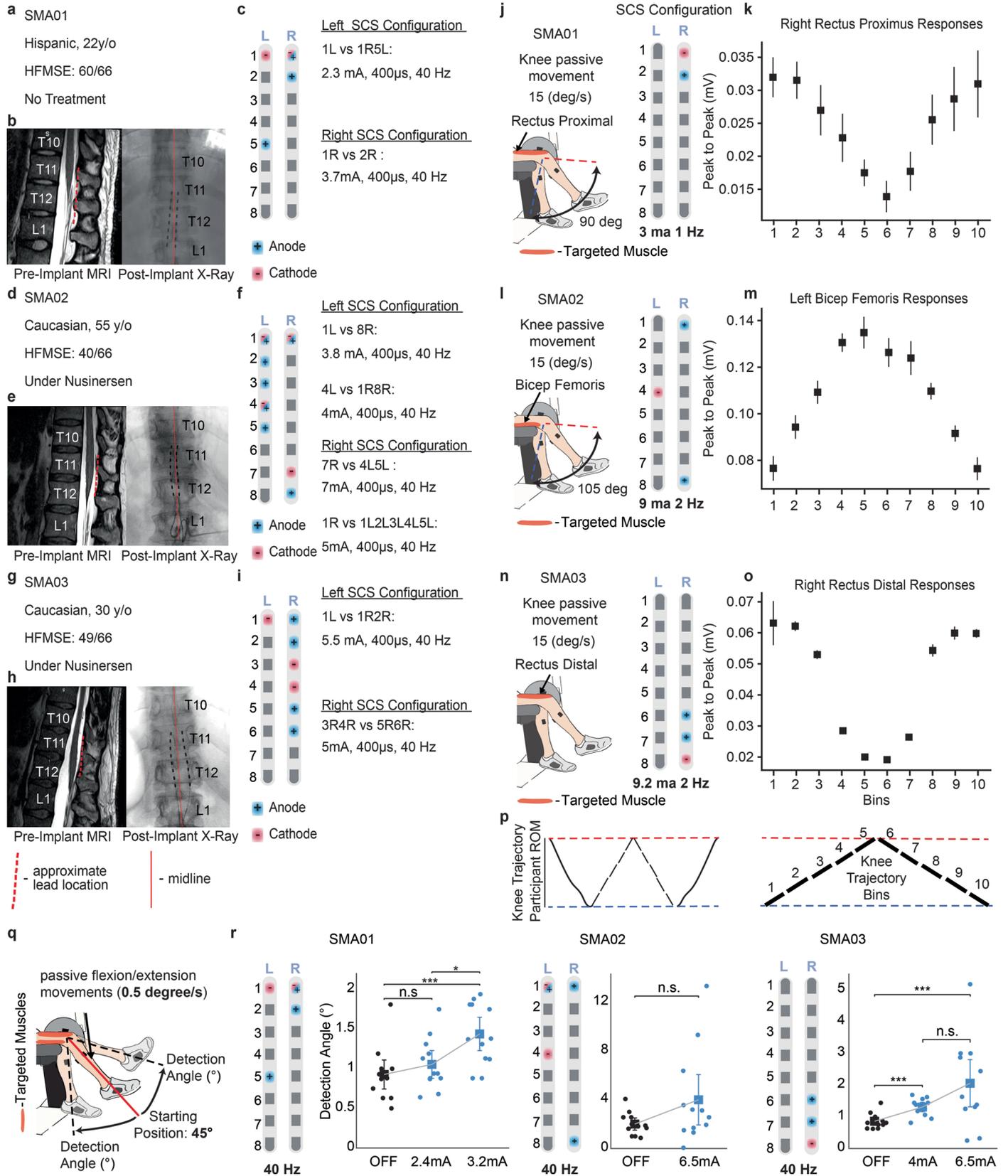
Extended Data Fig. 2 | See next page for caption.

Extended Data Fig. 2 | Implants, SCS configurations and effect of SCS on the natural modulation of sensory-motor circuit during passive movements. **a**, **d**, **g**, For each study participant demographic information, including ethnicity, age, score at the enrollment on the Hammersmith Functional Motor Scale Expanded (HFMSE), and detail on any treatment used. **b**, **e**, **h**. Left: pre implant T2 MRI, with the approximate lead location in red. Right: X-ray post-implant, with the bilateral leads in black. All three participants had the conus medullaris under the vertebra T12, a vertebra above what is normally observed (L1) **c**, **f**, **i**, SCS parameters used during walking. We used a program targeting the right and a program targeting the left leg muscles. Each program applied a fixed amplitude, frequency and pulse width for each SCS pulse. **j**, **l**, **n**. Configurations of the experimental set ups for passive knee joint movement for all participants and the SCS parameters used (anode blue, cathode red). **k**, **m**, **o**. Muscle responses were used to compute the peak to peak of each bin. Plots are reporting the

mean and 95% CI of the peak-to-peak responses. All error bars indicate the confidence interval, computed with bootstrap (N = 10,000). **p**. The cycle of joint oscillations was divided into 10 bins of equal duration during which the muscle responses were extracted and regrouped. **q**. Configuration of the experimental set up for proprioception testing (Supplementary Methods). Randomly selected flexion or extension movement were imposed to the knee joint of each subject at a speed of 0.5 degree per second. **r**. Configurations of SCS parameters used (anode blue, cathode red) and the detection angle (the difference between the starting angle and final angle displacement) plotted for each participant under varying SCS conditions of the proprioception testing: SCS OFF (black), SCS ON (light blue). The SCS ON condition was continuous stimulation at 40 Hz. Statistical differences were assessed with two-sided bootstrap (N = 10,000). *, **, and *** denote significant differences with p-values of p < 0.05, p < 0.01, and p < 0.001, respectively.
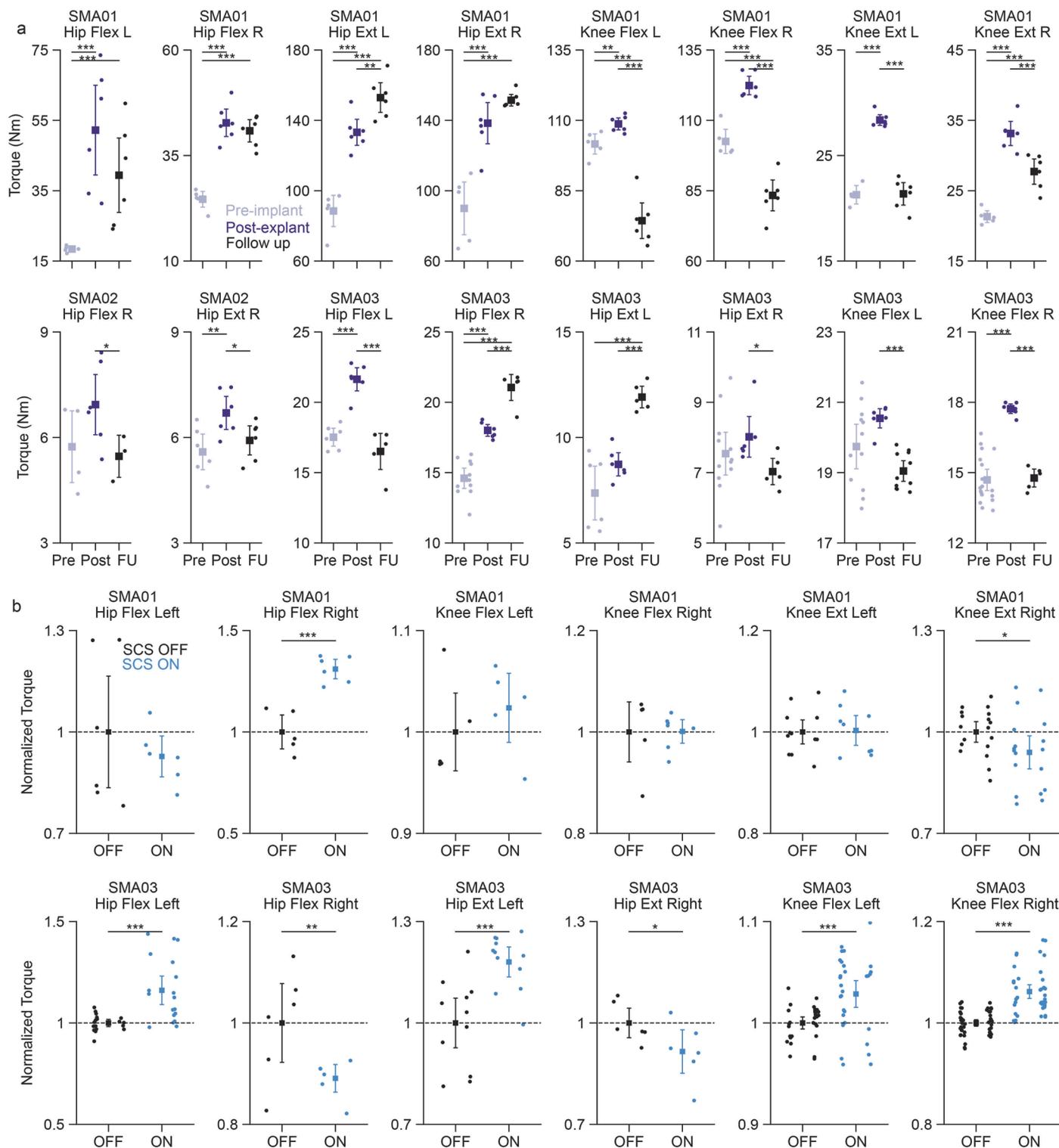
Extended Data Fig. 3 | Therapeutic and assistive effects in maximum torque. **a,** Maximum strength in hip and knee for all participants at pre-implant, post-explant and follow up (6 weeks after post explant). To reduce the day-to-day variability in our measures of maximum torque, we used data from all session's pre-implant and post-explant (see Extended Data Fig. 4b–f). We corrected for multiple comparison using Bonferroni with N = 3 (pre-implant vs post-explant, pre-implant vs follows up and post-explant vs follow up) **b,** Maximum strength with SCS ON and OFF for all sessions normalized by the mean maximum torque with SCS OFF across repetitions for of each session. Error bars show the mean and 95% confidence interval of the mean, computed with bootstrap (N = 10,000). Each dot represents the torque of a single repetition. All statistical significance was assessed with two-sided bootstrapping (N = 10,000): p < 0.05 (*), p < 0.01 (**), p < 0.001(***).
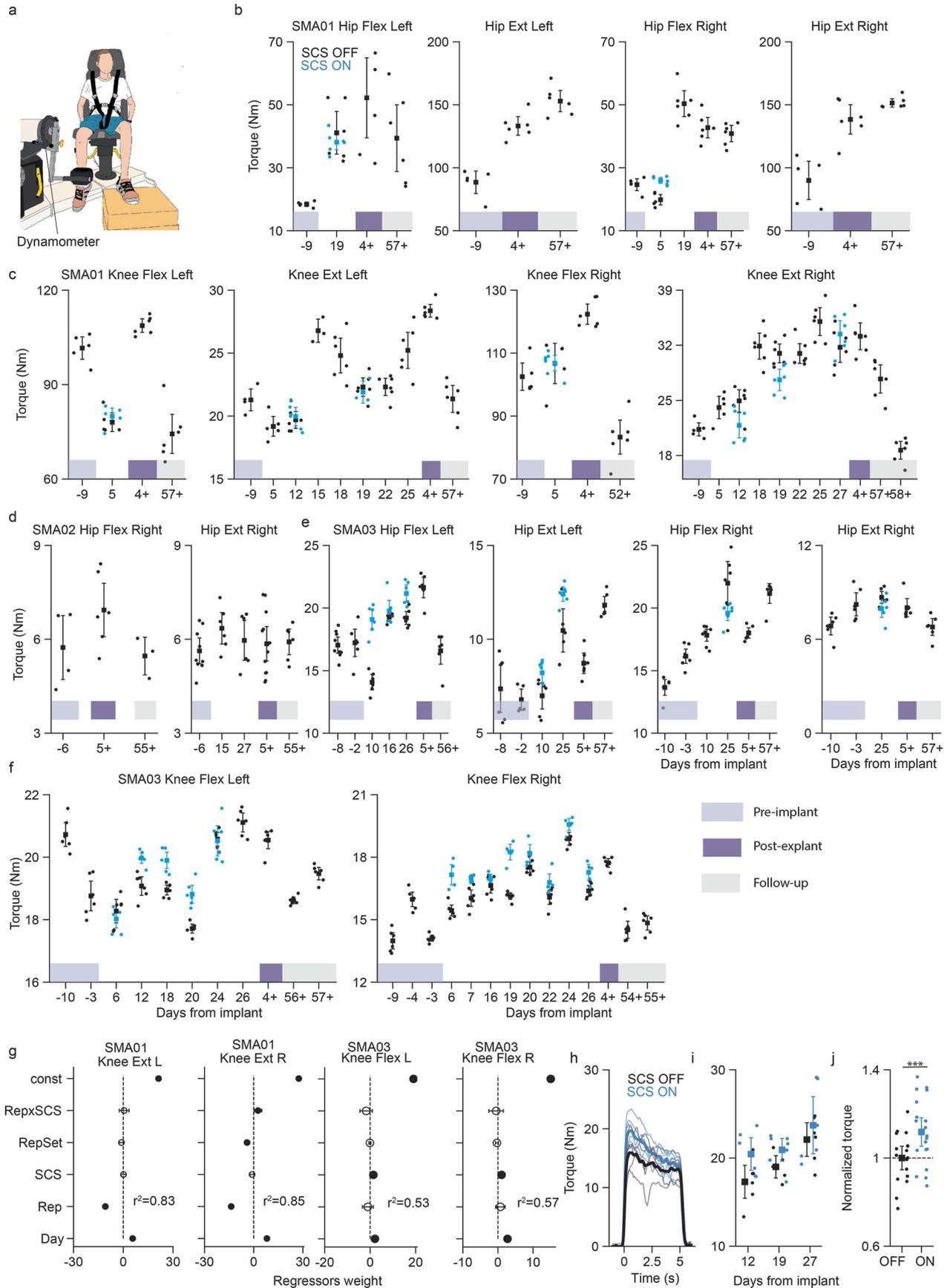
Extended Data Fig. 4 | See next page for caption.

Extended Data Fig. 4 | Torque raw data for all joints, functions and subjects and effect of fatigue in maximum torque. a, Experimental set up to measure isometric torques for knee extension and flexion. **b-f** Maximum voluntary contraction in all muscles, sessions and subjects that we could reliably measure (torque above 4 N): SMA01 Hip (**b**), SMA01 Knee (**c**), SMA02 Hip (**d**), SMA03 Hip (**e**) and SMA03 (**f**). Each point corresponds to one repetition and the square represents the mean across repetitions. **g**, We used a multivariable linear regression analysis to study the effect of fatigue in our measurements of torque (see Methods). For SMA01, we found that the largest regressor was the repetition indicating that SMA01 was fatiguing after only a few repetitions of maximum voluntary contractions. Given that we always started with SCS OFF trials, our results could be underestimating the assistive effect of SCS (Fig. 3a-c). Indeed,

we found for SMA01 right knee extension, the interaction between the SCS and the repetition number was significant indicating that SCS increased maximum torque when SMA01 was fatigued. In SMA03 we reduced the trial duration time from 5 to 2 seconds and we found that the repetition number had no impact indicating that direct comparison between SCS OFF and ON trial is probably not affected by the repetition number. **h**, Torque traces for SCS ON and SCS OFF fatigued repetition (after more than 12 repetitions of maximum voluntary contraction) in day 12 (See supplementary methods for more information). **i**, Maximum torque at right knee extension produced by SMA01 in fatigued trials for each session. **j**, Data from all sessions pooled where we tested the maximum torque in fatigued condition. All error bars show the mean and 95% confidence interval of the mean, computed with bootstrap (N = 10,000).
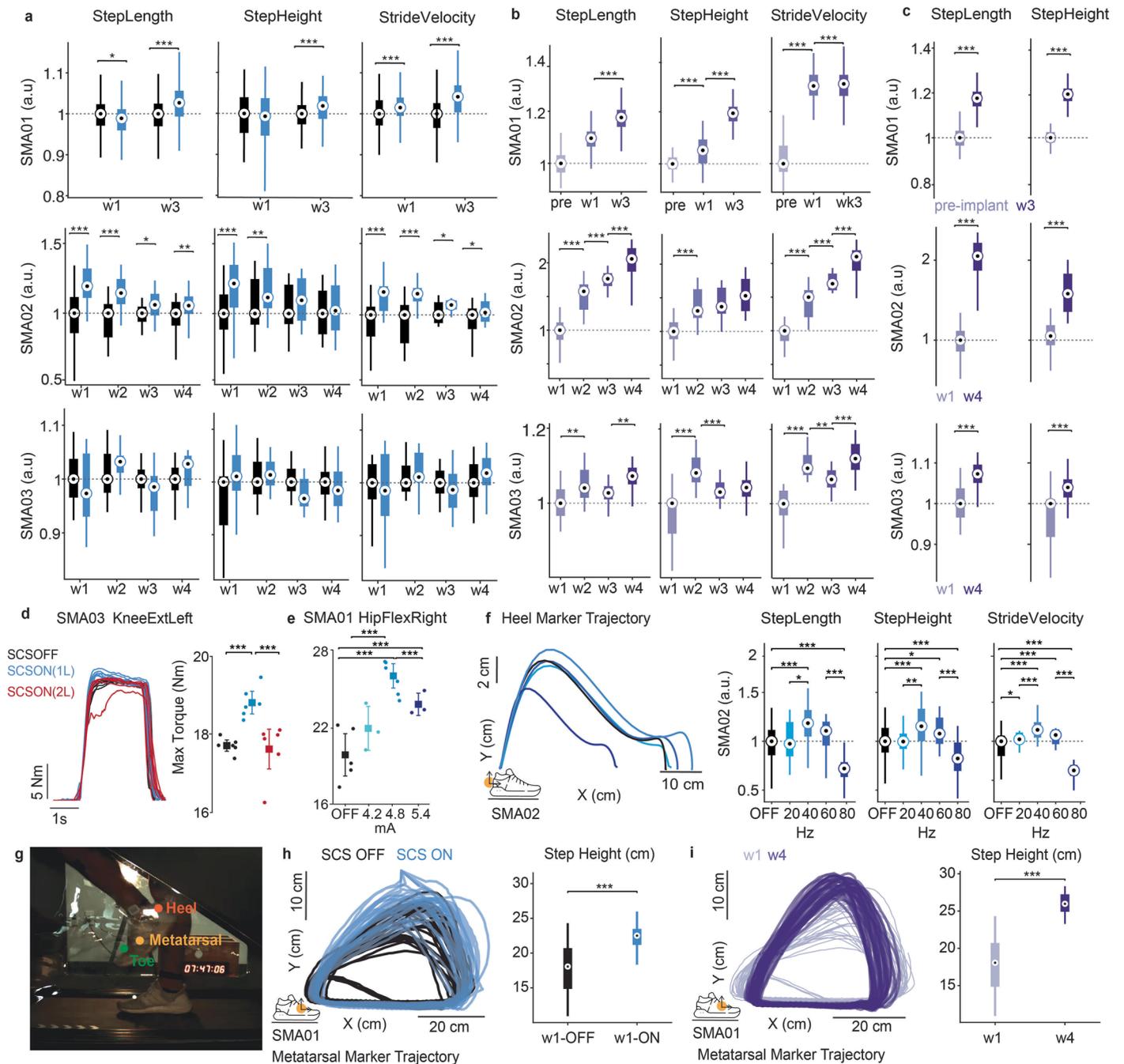
Extended Data Fig. 5 | Gait and Sham. a. Gait variables (step length, step height, and stride velocity) for SCS ON and OFF for all sessions normalized by the median value with SCS OFF across repetitions for each session. P-values corrected with Bonferroni correction (N = 2, 4 and 4 for SMA01, SMA02 and SMA03 respectively) **b**, Same gait variables for each session with SCS OFF. We used Kruskal Wallis ANOVA to find significance differences between groups (all p-values < 0.001). To study if the improvements saturated, we compared each week with the following week. In most gait quality variables, the improvements do not saturate (significance difference between week 3 and week 4). P-values corrected using Bonferroni correction (N = 3, 4 and 4 for SMA01, SMA02 and SMA03 respectively) **c**, Therapeutics effects in gait quality variables (week 1 vs week 4). All gait quality variables improved after the SCS intervention. **d.** Left, Examples of isometric torque traces during maximum voluntary knee extension contraction with SCS ON, SCS OFF, and with sham SCS parameters. The sham consisted of an SCS configuration chosen not to target the specific muscles involved in the joint movement tested changing the active contacts or the amplitude or frequency of the stimulation. Right, Maximum torque during knee extension for SCS ON,

OFF, and sham SCS parameters. Dots represent individual repetitions, while error bars indicate mean and the 95% CI of the mean (CI). **e.** Maximum torque during Hip Flexion for SMA01 using the same program with different stimulation amplitudes. Dots represent individual repetitions, while error bars indicate mean and the 95% CI of the mean (CI). **f.** Left, Mean heel marker trajectory across gait cycles with SCS ON using same program and different frequencies. Right, gait quality variables computed under the same conditions. P-values corrected using Bonferroni correction (N = 7). **g**, Setup for testing exaggerated hip flexion walking on the anti-gravity treadmill (Supplementary Methods). **h**. Left, Examples of metatarsal marker trajectory during exaggerated hip flexion walking with SCS ON and OFF. Right, The maximum hip flexion increased with SCS ON. **i**, same to **h**, considering SCS OFF in week 1 vs week 4. Again, the maximum hip flexion increased from week 1 to week 4 even without SCS. Box plots represent the median, 25th and 75th percentile and minimum and maximum data points without outliers. All statistical significance was assessed with two-sided bootstrapping (N = 10,000) and corrected for multiple comparisons: p < 0.05 (*), p < 0.01 (**), p < 0.001(***).
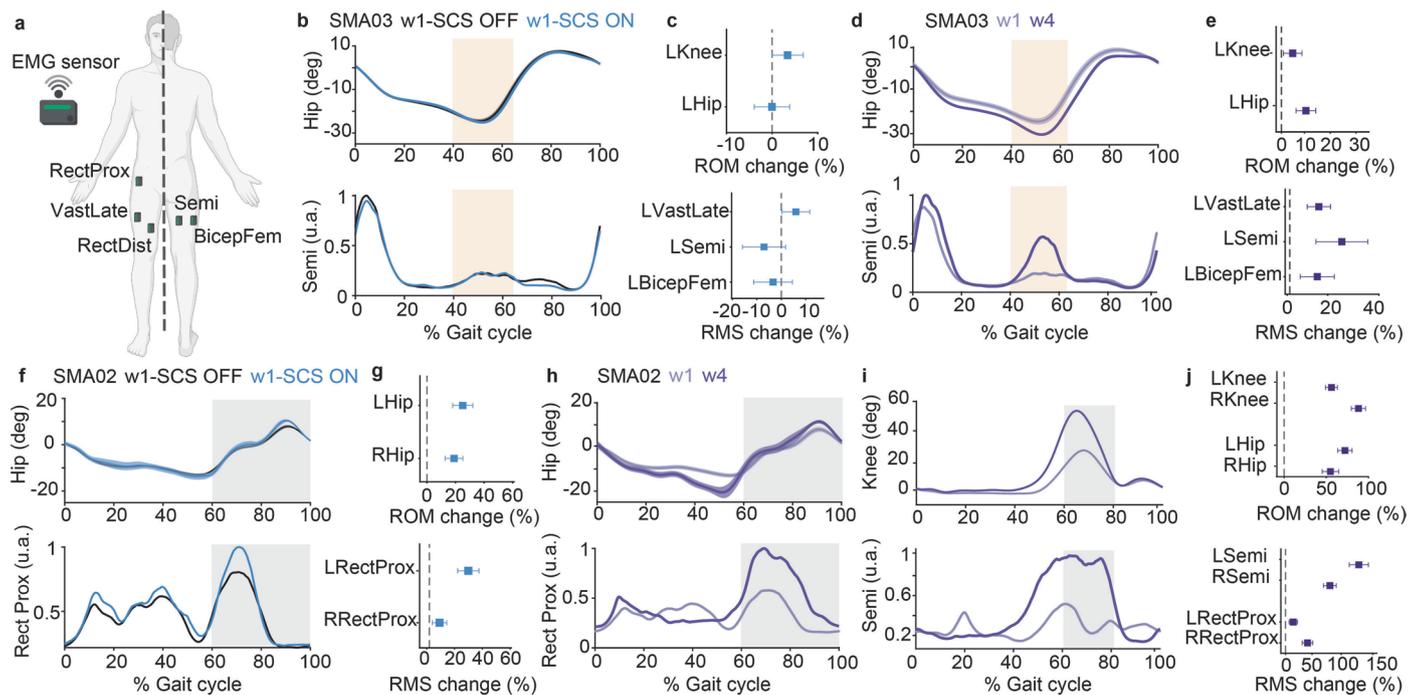
Extended Data Fig. 6 | Increases in range of motion are paralleled by increases in EMG activity. a. Scheme depicting the placement of the EMG sensor during overground walking (Supplementary Methods). **b-c** Assistive effects in range of motion (ROM) for SMA03 during week1. **b**, Top: Mean of hip flexion/extension across gait cycles with SCS OFF (black) and SCS ON (light blue). Bottom: Mean envelope of Semitendinosus (Semi) across the gait cycle with SCS OFF (black) and SCS ON (light blue). The gold shades highlight semitendinosus activation in the pre-swing, contributing to hip extension during the same phase of the cycle. **c**. Top: Mean change in ROM for the left hip and knee across gait cycles (n = 18, SCS ON; n = 17 SCS OFF). Bottom: Change in EMG activity, computed as the root mean square, for Semitendinosus (Semi), Vastus Lateralis (VastLate), and Biceps Femoris (BicepFem). Improvements in hip ROM should be correlated with the EMG activity at Semi and BicepFem (muscles involved in hip extension). Improvements in knee extension should be related to higher activation on the knee extensors. No change of EMG or ROM. **d-e** Mean therapeutic improvement in ROM during a gait cycle for SMA03 (n = 17, week 1; n = 16 week 4). Improvements in hip and knee ROM are paralleled by an increase in EMG activity at hip and knee extensors. **f-g**. Mean assistive improvement in ROM during a gait cycle (n = 60 SCS OFF; n = 28 SCS ON) for SMA02 in week 1. The gray shades highlight Rectus Femoris proximal activation in the swing phase, contributing to hip flexion during the same phase of the cycle. An increase in hip ROM can be explained by an increase in EMG activity at the Rectus Femoris proximal (a proxy of EMG activity of the hip flexors such as the iliopsoas). **h-j**. Therapeutic improvement in ROM during a gait cycle (n = 60, week 1; n = 18 week 4) for SMA02. Improvements in hip and knee ROM are correlated with increases in EMG activity of hip flexors (rectus femoris proximal) and knee flexors (Semi) No data is reported for SMA01 due to EMG acquisition corruption by noise. Error bars show the mean and 95% confidence interval of the mean, computed with bootstrap (N = 10,000).

a

PtID	HFMSE			6MWT		
	PreImpl	PostExpl *	FollowUp	PreImpl	PostExpl	FollowUp
SMA01	60	61 (+1)	61 (+1)	519	552 (+33m)	500 (-19m)
SMA02	40	40	43 (+3)	72	92 (+20m)	93.5 (+21.5m)
SMA03	49	49	49	102	126 (+24m)	106 (+4m)

*For SMA02 and SMA03 the HFMSE PostExpl was acquired the day of the explant
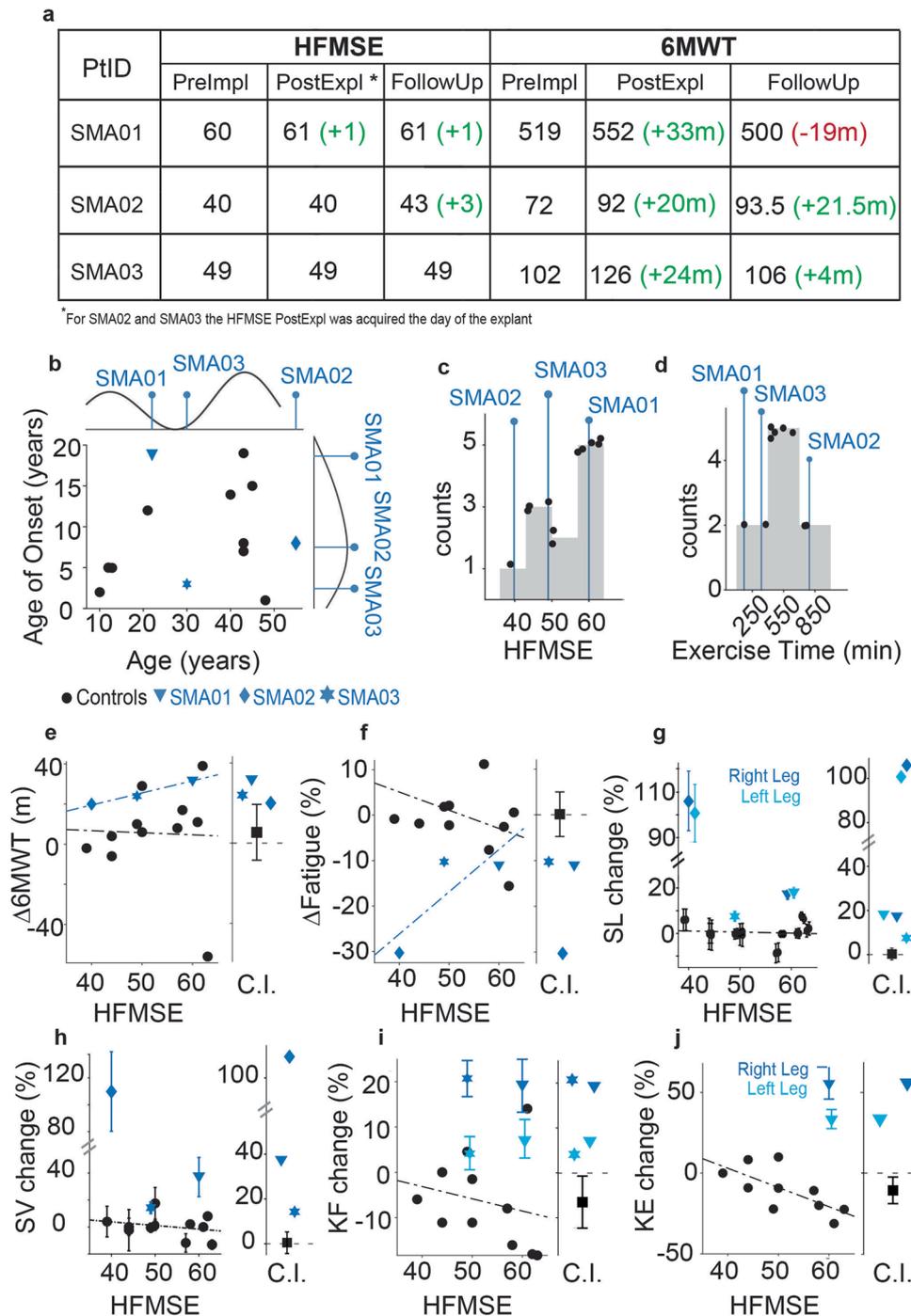
Extended Data Fig. 7 | Comparison with the full dataset of exercise-only controls. Comparison with all exercise-only control participants who completed three months of aerobic and strength training, including 3 minors. Changes for the control group were computed by comparing pre- and post- 3 months exercise intervention data, while changes for the SCS group were computed by comparing pre-implant and post-explant data, except otherwise specified. **a**, Clinical assessments. HFMSE and 6MWT measured pre-implant, post-explant and 6 weeks follow up. In parenthesis changes from baseline measures. All tests executed with SCS OFF. 6MWT dropped back to pre-implant at 6 weeks follow up in 2/3 participants. **b**, Relationship between age and age of onset for exercise-only control group (black) and the participants in our study (blue). **c**, Histogram of HFMSE scores for the control group (black), blue lines represent the HFMSE scores for each SCS participant. **d**, Histogram of aerobic exercise time for the control group (black), and exercise time of each SCS participant (blue lines). **e**, left: Relationship between the change in 6MWT score and the HFMSE score for the controls ($R^2 = 0.001$) and the SCS participants ($R^2 = 0.98$). Right: Mean and 95%CI of the mean change in 6MWT score for the controls (black) and changes for SCS participants (blue). **f**, Left: Linear regression analysis between the change in fatigue index during the 6MWT and the severity for both the control group ($R^2 = 0.15$) and the SCS participants ($R^2 = 0.7$). Right: Mean and 95% CI of the mean change in fatigue index across controls (black) and changes for SCS participants (blue) **g**, left: Regression analysis between the change in stride length and severity for controls ($R^2 = 0.01$), blue dots indicate SCS participants. Right: Mean change in stride length for the controls (black), and changes for SCS participants (blue). **h**, Same as g for stride velocity ($R^2 = 0.07$). For the SCS participants, changes were computed during self-paced overground walking, comparing SCS OFF trials from week 1 and week 4. **i**, Left: Regression analysis between the change in knee flexion strength for the controls ($R^2 = 0.05$). Improvements for SMA01 and SMA03 and their confidence intervals are shown in blue. Right: Mean knee flexion strength for the controls (black) and SCS participants (blue). **j**, Same as i for knee extension ($R^2 = 0.48$). Error bars represent the 95% confidence interval of the mean, computed with bootstrapping (N = 1000).
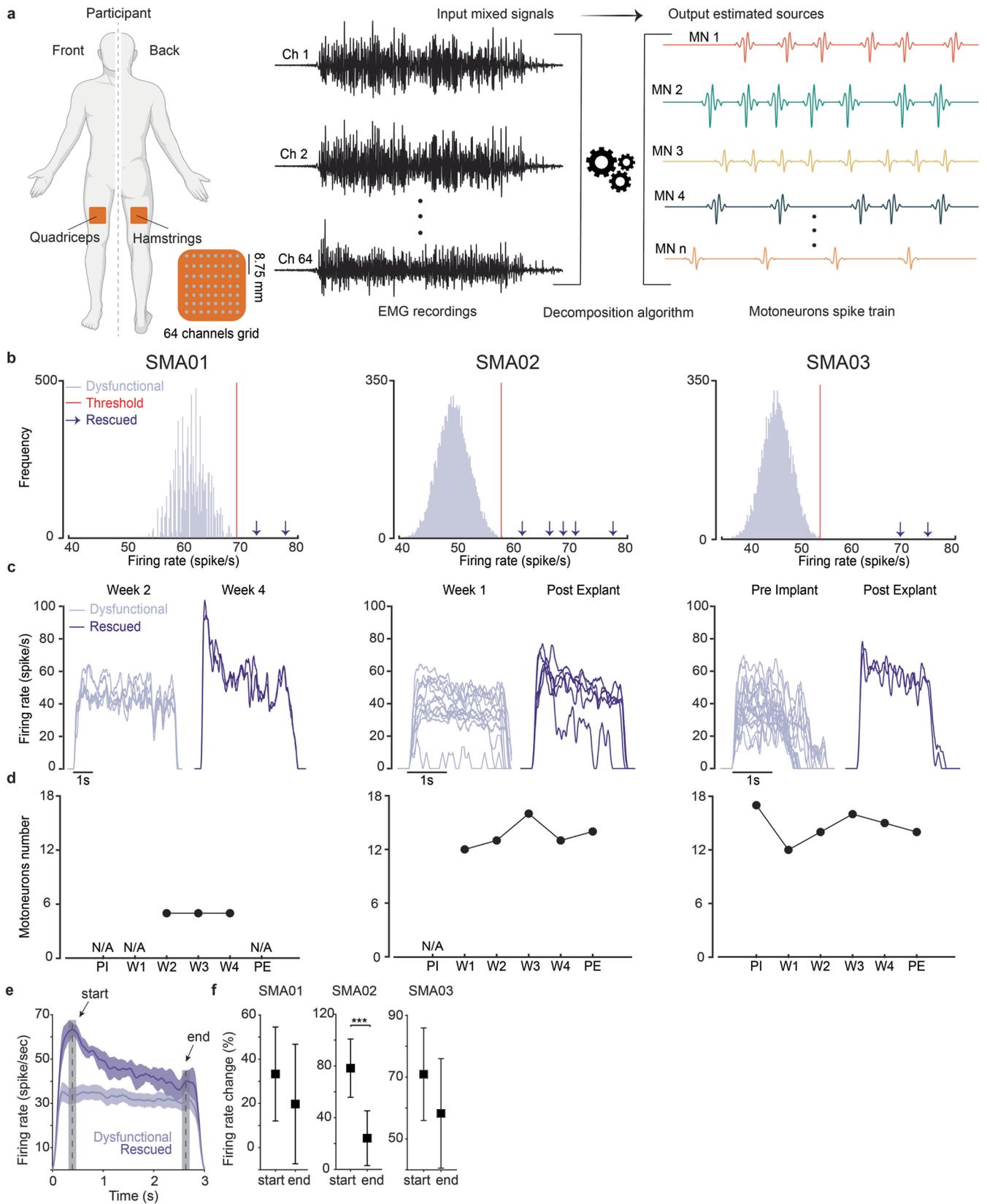
Extended Data Fig. 8 | See next page for caption.

Extended Data Fig. 8 | High Density EMG decomposition in single motor units spike trains. a. Pipeline to extract single motor units spike trains from high density surface electromyography (HDEMG). We used an 8 × 8 channel flexible grid to record muscle activity from both knee extensor (Rectus Femoris (RF)) and flexor (Biceps Femoris (BF)). Participants performed two sets of three isometric Maximum Voluntary Contractions (MVC) of knee extension and flexion. We used the convolution kernel compensation (CKC) method to decompose the EMG signals in single motor units spike trains. **b**. Rescued motoneuron identification: a motor unit was defined as rescued if its mean peak firing rate (across trials) was higher than the 99.73 % CI (red line) of mean peak firing rate across motor units recorded during the first session. The 99.73% CI was computed with bootstrap (N = 10,000). **c**. Example of motor units smoothed discharge rate (SDR) obtained during the 3rd MVC. Each line represents the SDR of every motoneuron. Light and dark colors delineate the data from the first and last session where we performed the experiment **d**. Circles illustrate the number of identified motoneurons over the different phases of the study. (that is, PI = pre-implant; Wi = i-th week after the implant; PE = post-explant). **e**, Example (SMA02) of the mean and 95% CI of post-explant single motoneurons firing rates during MVC. In gray regions indicate the start and end windows used to compute firing rate at the beginning and the end of the MVC. **f**, Percentage change in the mean firing rate between rescued and dysfunctional motoneurons at the start (first 150 ms) and end (last 150 ms) of the MVC for each participant. 95% CI were computed using bootstrapping (n = 10,000). We assessed statistical significance using a two-sided test with bootstrapping (n = 10000). Asterisk *, **, and *** denote significant differences with p-values of p < 0.05, p < 0.01, and p < 0.001, respectively.

Step 1

Recruitment of motor neurons using active mobilization of the knee joint to elicit neural activity in the spinal cord

Step 2
T2 and Raw 4D volume acquisition

Step 3
Define Spinal Segments from T2

Step 4
Motion Correction (3D and 2D, slice by slice)

Step 5
Automatic Segmentation (With Manual Corrections)

Step 6
Registration of 2nd and 3rd runs to 1st

Step 7
Co-registration between functional and PAM50 Template

Step 8
Application of General Linear Model to denoise physiological signals and then model task activation

Step 9
Apply Warping Fields (step 7) to Activity Patterns for PAM50

Step 10

Activity patterns resulting from General Linear Model analyses co-registered to PAM50 and analyzed for specific spinal segment (L1-S2)
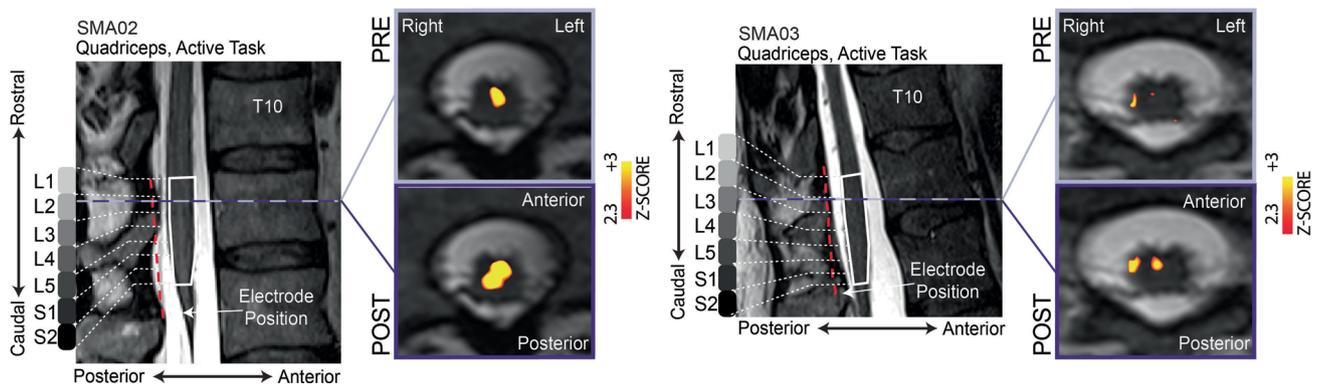
Extended Data Fig. 9 | See next page for caption.

Extended Data Fig. 9 | fMRI to detect spinal motoneuron function. Step 1, Acquisition of functional MRI from the spinal cord in response to the recruitment of motor neurons from specific leg muscles. The motor neurons are recruited by actively extending and flexing the knee joint. Three runs are acquired for each participant. Only the right leg muscles are tested. Instructions were displayed on a screen (fixation cross '+' during rest blocks and text indicating activity blocks), while auditory cues were used to signal changing phases. In addition to the functional volume series, T2 anatomical images and physiological (heart rate, respiratory) signals are acquired. Step 2, Raw fMRI volume series are repeatedly acquired every 2.5 s (TR) in functional runs lasting about 6 minutes. Step 3, Spinal segments are identified from high-definition T2-ZOOMit structural images, T2 images and SCS recruitment curve responses. Spinal segments are then reported in the T2 anatomical image acquired in each run. Step 4, Then motion correction is applied to each functional run in two stages. First, volumes are aligned to the averaged images using 3D rigid body realignment. Second, a slice-by-slice 2D realignment is applied to each volume. Step 5, The spinal cord (including gray and white matter) is automatically segmented from the motion corrected mean functional image, and then manually corrected. Step 6, Functional images from runs two and three are aligned to functional images of run one using the motion corrected mean images by landmarking the conus medullaris and any visible vertebra, using rigid transformations. Step 7, The motion corrected mean images are then coregistered to the PAM50 template using the conus medullaris landmark to extract the transformation matrices, using non-rigid transformations. Step 8, Physiological signals (heart rate and respiratory) acquired concomitantly to the fMRI volumes are used to model physiological noise (RETROICOR based procedure). Acquisition timings corresponding to motion corrected fMRI volume series and physiological noise regressors are submitted to a specific first level generalized linear model (GLM). Residuals from this GLM are then spatially smoothed, volume by volume with 3D gaussian kernel with full width at half maximum (FWHM) of 2x2x6mm3. Acquisition timings corresponding to the task-design and residuals resulting from noise removal are submitted to a specific first level GLM. A second level fixed effects analysis (subject level, task specific) is performed by combining the three runs. Activity pattern maps are uncorrected and thresholded (Z > 2.3, p < 0.01). **Step 9**, Transformations matrices found in step 7 are then applied to the resulting activity pattern maps of step 8 to arrive in PAM50 space. **Step 10**, Activity patterns from the three participants, are then compared and analyzed across scanning sessions using the spinal segments found in step 3.
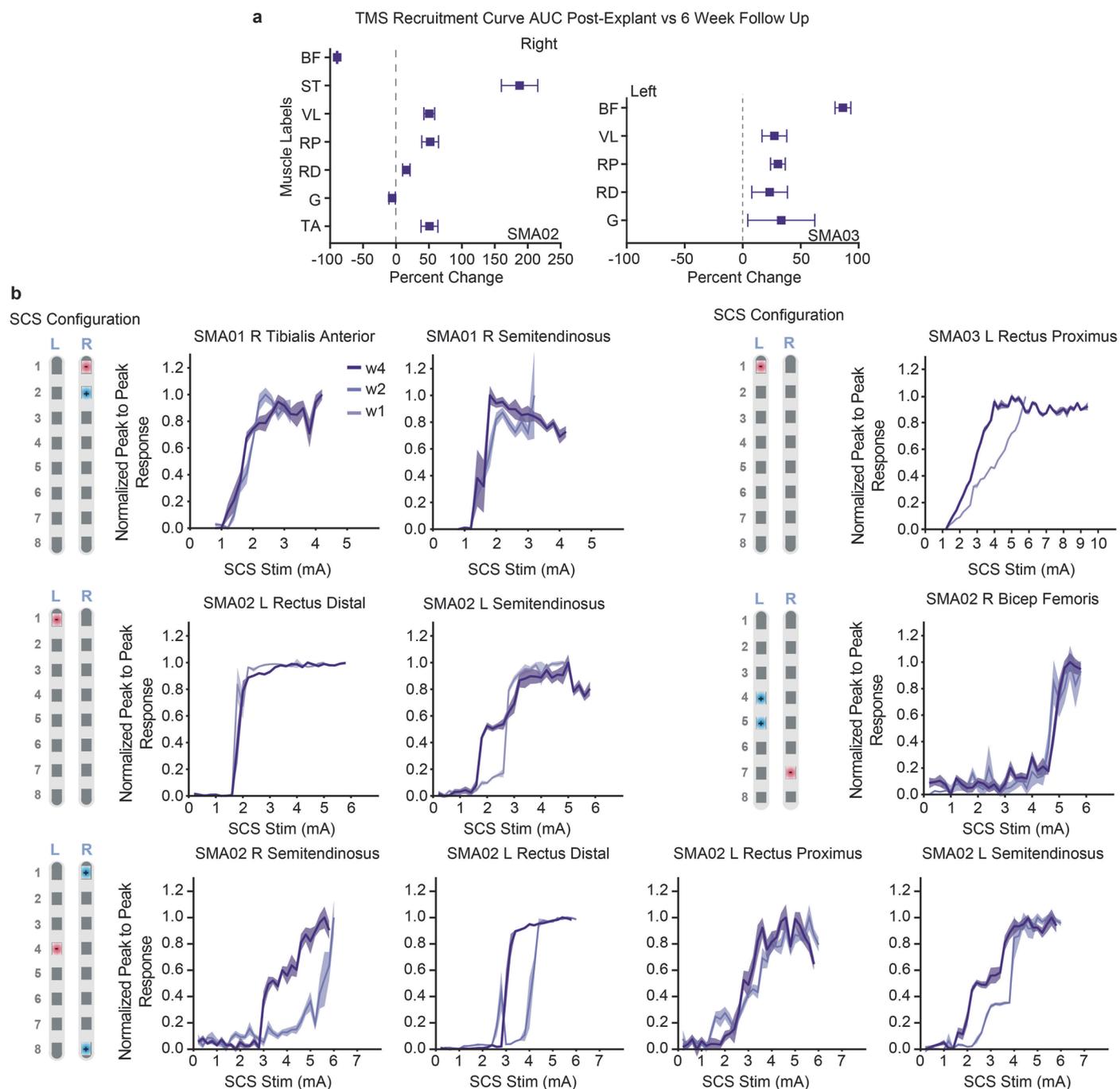
Extended Data Fig. 10 | Assessment of spinal cord stimulation induced responses. a, Quantification of percent change in area under the curve of peak-to-peak TMS responses post-explant vs six week follow up across all intensities tested. Abbreviations: ST, Semitendinosus; BF, Bicep Femoris; VL, Vastus Lateralis; RP, Rectus Femoris Proximal; RD, Rectus Femoris Distal; G, Gastrocnemius; TA, Tibialis Anterior. Error bars are the mean and 95% CI of the mean peak-to-peak responses (bootstrap N = 10,000). **b**, The SCS parameters used and the resulting plots representing the normalized peak-to-peak response as a function of SCS amplitude. Shaded areas correspond to standard error across responses, while thick lines are the means across responses.

Corresponding author(s): Marco Capogrosso, Elvira Pirondini, Robert M. Friedlander

Last updated by author(s): Nov 22, 2024

Reporting Summary

Nature Portfolio wishes to improve the reproducibility of the work that we publish. This form provides structure for consistency and transparency in reporting. For further information on Nature Portfolio policies, see our Editorial Policies and the Editorial Policy Checklist.

Statistics

For all statistical analyses, confirm that the following items are present in the figure legend, table legend, main text, or Methods section.

n/a	Confirmed	
☐	☒	The exact sample size (*n*) for each experimental group/condition, given as a discrete number and unit of measurement
☐	☒	A statement on whether measurements were taken from distinct samples or whether the same sample was measured repeatedly
☐	☒	The statistical test(s) used AND whether they are one- or two-sided *Only common tests should be described solely by name; describe more complex techniques in the Methods section.*
☐	☒	A description of all covariates tested
☐	☒	A description of any assumptions or corrections, such as tests of normality and adjustment for multiple comparisons
☐	☒	A full description of the statistical parameters including central tendency (e.g. means) or other basic estimates (e.g. regression coefficient) AND variation (e.g. standard deviation) or associated estimates of uncertainty (e.g. confidence intervals)
☐	☒	For null hypothesis testing, the test statistic (e.g. *F*, *t*, *r*) with confidence intervals, effect sizes, degrees of freedom and *P* value noted *Give P values as exact values whenever suitable.*
☒	☐	For Bayesian analysis, information on the choice of priors and Markov chain Monte Carlo settings
☒	☐	For hierarchical and complex designs, identification of the appropriate level for tests and full reporting of outcomes
☒	☐	Estimates of effect sizes (e.g. Cohen's *d*, Pearson's *r*), indicating how they were calculated

Our web collection on statistics for biologists contains articles on many of the points above.

Software and code

Policy information about availability of computer code

Data collection	Data collection
	Data were collected using the following software: custom MATLAB R2020a/b and R2021a/b code interfacing with an NI Data Acquisition Board (PCI-6255) and an interprocess communication framework written in MATLAB (Dragonfly; Velliste,3013) for synchronously recording stimulus pulse timing, EMG, and experimental performance parameters, We used the HUMAC2015 v15.000.0276 (HUMAC NORM) software environment for collecting joint torque data, and VICON Nexus 2.12.1 for acquiring 3D kinematics during locomotion. Kinematics during treadmill walking was captured using a GoPro® Camera and analyzed the data with Deeplabcut(v 2.3.8). Intra- operative CMAPs were recorded using EPWorks software running on the XLTEK Protektor32 (Natus). MRI of the lumbosacral spine was acquired using a 3T MRI scanner (Magnetom Prismafit, Siemens Healthineers) with a 32-channel spine array coil. The biophysical model was developed using Python 3.9 and the Neuron library. Code available: https://github.com/genisprat/BiophysicalModel_SCSinSMA. HD-EMG data were collected using the TMSI system

| Data analysis | Data analysis of all kinematics, joint torque, electromyography, functional performance, recruitment curve, and clinical assessments were performed using custom analysis code written in MATLAB R2022b and R2023a/b and Python 3.9. Data from intra-operative electrophysiology were extracted manually from proprietary data files using the EPWorks v6.1.2.38 software (Natus). The fMRI pre-processing utilized the FMRIB Software Library (FSL) v6.06 and the Spinal Cord Toolbox (SCT) v6.1.All figures were rendered in Adobe Illustrator CC v26.0-26.3.1 |

For manuscripts utilizing custom algorithms or software that are central to the research but not yet described in published literature, software must be made available to editors and reviewers. We strongly encourage code deposition in a community repository (e.g. GitHub). See the Nature Portfolio guidelines for submitting code & software for further information.

Data

All manuscripts must include a data availability statement. This statement should provide the following information, where applicable:

- Accession codes, unique identifiers, or web links for publicly available datasets
- A description of any restrictions on data availability
- For clinical datasets or third party data, please ensure that the statement adheres to our policy

The data that support the findings of this study are openly available at: 10.5281/zenodo.14201208. To protect confidentiality of participants, raw data requests should be made officially to MC or RMF. Reasonable requests for data will be fulfilled upon IRB approval via official material transfer agreements between the University of Pittsburgh and the requesting party taking into account any existing sponsored research contract agreements with the funders.

Research involving human participants, their data, or biological material

Policy information about studies with human participants or human data. See also policy information about sex, gender (identity/presentation), and sexual orientation and race, ethnicity and racism.

Reporting on sex and gender	In this study all three participants were of the sex male and all three participants self-identified as male gender. Sex based analysis was not appropriate for this study, due to low sample size.
Reporting on race, ethnicity, or other socially relevant groupings	In this work we report results from the first 3 participants in our trial where SMA01 was a hispanic male and SMA02 and SMA03 were caucasian males. These were self-reported by the participants. Race based based analysis was not appropriate for this study.
Population characteristics	SMA01 (22 years) was diagnosed with 5q-autosomal recessive Spinal Muscular Atrophy (SMA) type III confirmed through genetic testing for a deletion in the SMN1 gene (5q12.2-q13.3). He had mild motor deficits with an HFMSE at enrollment of 60/66 points. He was not under any treatment during the duration of the study

SMA02 (55 years) was diagnosed with 5q-autosomal recessive Spinal Muscular Atrophy (SMA) type III confirmed through genetic testing for a deletion in the SMN1 gene (5q12.2-q13.3). He had severe motor deficit with HFMSE at enrollment of 38/66 points. During the study he was under Nusinersen.

SMA03 (30 years) was diagnosed with 5q-autosomal recessive Spinal Muscular Atrophy (SMA) type III confirmed through genetic testing for a deletion in the SMN1 gene (5q12.2-q13.3). He had moderate motor deficit with HFMSE at enrollment of 38/66 points. During the study he was under Nusinersen. |
| Recruitment | The study was advertised through SMA patients associations, cure-SMA and SMA Europe . Subjects signed an informed consent whose content were approved by the IRB of the University of Pittsburgh. SMA02 was recruited through referral via collaborator, SMA01 and SMA03 contacted the study via the Pitt+me platform of the University of Pittsburgh. As there was only one study group, recruitment was not subject to self-selection bias. |
| Ethics oversight | All experimental protocols were approved by the University of Pittsburgh Institutional Review Board (Protocol STUDY21080158) under abbreviated IDE. Our study is published on ClinicalTrial.gov number NCT05430113 |

Note that full information on the approval of the study protocol must also be provided in the manuscript.

Field-specific reporting

Please select the one below that is the best fit for your research. If you are not sure, read the appropriate sections before making your selection.

☒ Life sciences   ☐ Behavioural & social sciences   ☐ Ecological, evolutionary & environmental sciences

For a reference copy of the document with all sections, see nature.com/documents/nr-reporting-summary-flat.pdf

Life sciences study design

All studies must disclose on these points even when the disclosure is negative.

Sample size	No statistical methods were used to pre-determine sample sizes. All data was analyzed in all subjects independently and no formal statistical comparison between populations was performed. Data comes from the first three enrolled subjects in our clinical trial and no other subject was excluded from the analysis. Number of specific data points and repetitions is similar to other studies using similar measures (Wagner 2018, Nature, Gill 2018 Nature Med, Powell 2022)
Data exclusions	Single joint torque measurements below 4 Nm were excluded because they were not reliable due to the biomechanical noise of our system. This was particularly important for SMA02 where we could only measure torque in his right hip. Instead, for SMA01, we could measure all joints and for SMA03 all joints except knee extension. I the control study (Montes 2015), we excluded one participant with
Replication	The reproducibility of experimental finding was confirmed across three subjects and across multiple sessions (assistive effects of stimulation

Replication	were assessed several times for each subject as reported in the manuscript) Due to the variability in the severity of the disease, some of the task where adapted for each participant.
Randomization	No randomization was introduced in our experiments. Since no formal statistical comparisons were required in our study and all participants were independently analyzed, no randomization was necessary and the same protocol was performed on all participants.
Blinding	Blinding was performed during HFMSE test on the examiner to whether stimulation was on or off. No other blinding was performed for experiments because participants were able to percived wether the stimulation was ON or OFF. Instead we performed sham experiments where we changed stimulation parameter and show that efficacy was dependent of the stimulation parameters.

Reporting for specific materials, systems and methods

We require information from authors about some types of materials, experimental systems and methods used in many studies. Here, indicate whether each material, system or method listed is relevant to your study. If you are not sure if a list item applies to your research, read the appropriate section before selecting a response.

Materials & experimental systems

n/a	Involved in the study
☒	☐ Antibodies
☒	☐ Eukaryotic cell lines
☒	☐ Palaeontology and archaeology
☒	☐ Animals and other organisms
☐	☒ Clinical data
☒	☐ Dual use research of concern
☒	☐ Plants

Methods

n/a	Involved in the study
☒	☐ ChIP-seq
☒	☐ Flow cytometry
☐	☒ MRI-based neuroimaging

Clinical data

Policy information about clinical studies

All manuscripts should comply with the ICMJE guidelines for publication of clinical research and a completed CONSORT checklist must be included with all submissions.

Clinical trial registration	NCT05430113
Study protocol	The full study protocol is available for viewing at ClinicalTrials.gov (NCT05430113)
Data collection	All surgical procedures were performed at UPMC Presbyterian Hospital in Pittsburgh, PA. All data were collected in the laboratories of Dr. Marco Capogrosso and Dr. George Wittenberg. Recruitment started on January 2022 until July 2023. Data collection start on September 2022 until July 2023. Ea ch subject came into the lab for 8 days of pre-implant testing during the 2 weeks leading up to the implant date. After the implant procedure, participants were given a full weekend to recover before data collection began. During the 30 day implant period, participants engaged in data collection for 4 hours per day on 5 days per week for a period of 4 weeks. Post-study follow up data collection was obtained in the laboratory 6 weeks following explant.
Outcomes	Primary Outcomes: Muscle Weakness, Isometric torque: measure the isometric torque produced by the subject at the hip during hip-flexion. Comparison of SCS-on with SCS-off performance. Success Criteria: ≥20% increased torque production over SCS-off baseline as measured during single-joint isometric torque. Number and Severity of Adverse Events Success Criteria: no serious adverse event related to the stimulation or intolerable adverse event reported. Secondary outcomes Muscle activation: measure surface EMGs produced by the subjects during isometric movements of the hip, knee, and ankle in the HUMAC Norm and compare SCS-on with SCS-off performances. Meaningful Change:<20% EMG RMS compared to SCS-on. Range of Motion (ROM): Meaningful Change: increase of >20% of the hip joint (if available) and the knee joint (if available) during SCS against SCS-off as measured by the HUMAC NORM during single-joint isotonic trials. Motor Function: 6 minute walk test: perform the 6-minute walk test with SCS-on and SCS-off and distance between SCS-on and SCS-off is set to 24 m. If not ambulator, any increased ambulation distance from SCS-off condition.

Motor Function Revised Hammersmith Functional Scale
The Revised Hammersmith Functional Scale is a further refined version of the Hammersmith Functional Motor Scale Extended and includes specific items focused on lower-limb motor control such as hip-flexion, standing and walking a that are particularly relevant for the type III population of study. The scale is a 36 item performance evaluation, with a score range from 0-69 in which higher scores indicate better performance. Meaningful Change: ≥2 point improvement. Compare outcomes between SCS-on and SCS-off. Motor Function Measure 32. The 32 items MFM is often used in trials of neuromuscular disorders, hence it provides a meaningful comparison against outcomes of other trials. Meaningful Change: ≥2 point improvement. Compare outcomes between SCS-on and SCS-off.

Motor Function: Fatigue
Fatigue will be assessed during motor function tests.

Discomfort/Pain
Patients will be asked to provide a score from 1 to 10 where a greater number indicates a greater amount of discomfort for each stimulation configuration. Spinal cord stimulation produces tingling sensations and other type of sensory phenomena. It is important to document that stimulation intensities required to improve motor function remain within a range of non-painful sensations.

Sensorimotor Network Structure Density
The investigators will perform High-definition Diffusion Weighted Imaging to quantify Fractional Anisotropy as a measurement of axon density in the brain and spinal cord pre and post study.

Impression
The investigators will collect subjects and therapist feedback on how the technology is performing and what they would want to modify using The Clinical Global Impression Scale, a scale of 1-7 where a lower number indicates better performance and a higher number indicates more greatly impacted by their disease.

Sensorimotor Network Structure Integrity The investigators will perform High-definition Diffusion Weighted Imaging to quantify Fractional Anisotropy as a measurement of axon integrity in the brain and spinal cord pre and post study.

Sensorimotor Network Function
The investigators will perform resting state and motor-task functional MRI of the brain and spinal cord to quantify neural network activation at rest and during the execution of simple motor task such as leg muscle contraction.

Cortico-spinal Tract Integrity
The investigators will measure muscle evoked potential consequent to Transcranial Magnetic Stimulation of the cortico-spinal tract to assess integrity of the cortico-spinal tract.

Spinal Circuit Excitability
The investigators will measure H-reflexes of leg muscles to quantify excitability of spinal motoneurons to stimulation of primary sensory afferents pre and post-study. Expected Result: Our main scientific hypothesis is that SCS will restore monosynaptic responses of weak spinal motoneurons, thus increasing H-reflex responses pre and post-study.

Motoneuron Firing Rates
The investigators will use high-density EMGs on leg muscles to calculate firing rates of single spinal motoneuron discharge during isometric maximal voluntary contractions.

Motor Firing Number
The investigators will use high-density EMGs on leg muscles to calculate the number of firing rates of single spinal motoneuron discharge during isometric maximal voluntary contractions.

Plants

Seed stocks	No seeds were used in this study
Novel plant genotypes	No novel plant genotypes used in this study
Authentication	No authentication needed as no plants were used in this study

Magnetic resonance imaging

Experimental design

Design type	task based with block design lumbar fMRI
Design specifications	SMA01 underwent three scan sessions (two pre-implant, and one post-explant). SMA02 and SMA03 underwent four

Design specifications	scan sessions (two pre-implant and two post-explant). Each session consisted of three runs of the task scan. Each run contained nine blocks of activity lasting 16 seconds each and a rest time between each block of 18-20 seconds.
Behavioral performance measures	No behavioral measures

Acquisition

Imaging type(s)	Structural and Functional
Field strength	3T
Sequence & imaging parameters	Structural scans consisted of a high-resolution sagittal T2-weighted SPACE sequence (single slab 3D turbo spin echo sequence with a slab selective, variable excitation pulse, repetition time (TR), 1500 ms; echo time (TE), 135 ms; voxel size, 0.4×0.4×0.8 mm3); and a 2D transverse T2-weighted SPACE with ZOOMit (dynamic excitation pulses to achieve selective/zoomed field-of-view) software (TR, 3080 ms; TE, 106 ms; voxel size, 0.9×0.9×0.5 mm3). Functional acquisitions were performed using a gradient-echo echo-planar sequence with a ZOOMit field-of-view imaging, with repetition time (TR), 2500 ms; echo time (TE), 34 ms; field of view (FOV), 48x144 mm; flip angle, 80°; voxel size, 1.0 x 1.0 x 3.0mm3; and 32 axial slices per volume
Area of acquisition	Thoracolumbosacral spinal cord. Ranging from T10 to to S2
Diffusion MRI	☐ Used ☒ Not used

Preprocessing

Preprocessing software	The fMRI pre-processing utilized the FMRIB Software Library (FSL) v6.06 and the Spinal Cord Toolbox (SCT) v6.17. The volumes of each run were averaged to create a mean functional image and was used to automatically detect the centerline of the spinal cord. A cylindrical mask (diameter of 30 mm) was generated along the centerline to prevent the inclusion of regions moving independently from the spinal cord. All runs corresponding to the same session were aligned to the first run of the session using three-dimensional rigid body realignment (spline interpolation and least square cost function). Both the cerebrospinal fluid and the spinal cord were automatically segmented (with manual corrections when necessary) using the Spinal Cord Toolbox (SCT) from the mean motion corrected functional images and the T2 anatomical images. Residuals were smoothed, volume by volume, using a 3D Gaussian kernel (with full width half maximum (FWHM) of 2 x 2 x 6 mm3, along the centerline of the spinal cord.
Normalization	Using the Spinal Cord Toolbox, functional images were coregistered to the PAM50 image with non-rigid transformations using the conus medullaris as landmarks to create functional-to-template warping fields.
Normalization template	PAM50 template
Noise and artifact removal	A two phase motion correction procedure was used. Using three-dimensional rigid body realignment (spline interpolation and least square cost function) all volumes within a run were registered to the mean image using FSL's MCFLIRT. Two-dimensional slice-wise realignment (spline interpolation and least square cost function) was performed with the mean functional image as the target. Noise regressors were generated using FSL's physiological noise modeling tool on the acquired cardiac and respiratory signals, with a procedure based on the RETROICOR. Low and high order Fourier expansions were used to model the physiological signals. Accordingly, we generated 32 noise regressors using the physiological noise modeling (PNM) tool from FSL, along with an additional regressor corresponding to the cerebrospinal fluid signal (10 % most variable cerebrospinal fluid voxels). The 33 physiological noise regressors, motion correction parameters (x and y), and motion outliers were regressed from the fMRI time-series using FSL's Expert Analysis Tool (FEAT).
Volume censoring	First 5 volumes were removed for signal stability. Motion scrubbing was employed to identify outlier volumes using FSL's outlier detection tool (DVARS metrics: root mean square intensity difference of volume N to volume N+1) within the spinal cord using a box-plot cut-off (75th percentile + 1.5 x the interquartile range).

Statistical modeling & inference

Model type and settings	We used the general linear model (GLM). As explanatory variables, the timings of the task (block design) were convolved with the three optimal basis functions using FMRIB's Linear Optimal Basis Set, with the second and third waveforms orthogonal to the first waveform. The resulting parameter estimates for the three runs were passed through a fixed-effects model to obtain the second level analysis (subject level and task specific).
Effect(s) tested	Changes in BOLD signal intensity based on modeling of task response vs rest comparing pre-implant to post-explant sessions
Specify type of analysis:	☒ Whole brain ☐ ROI-based ☐ Both
Statistic type for inference (See Eklund et al. 2016)	Testing for statistical differences of any GLM measure was done through bootstrapping method. A nonparametric approach that makes no distributional assumptions on the observed data. Bootstrapping instead uses resampling to construct empirical confidence intervals (Cis) for a quantity of interest. For each comparison we constructed bootstrap samples by drawing with replacement from the observed measurement. We calculated the null distribution of the observed difference by creating 10,000 bootstrap samples. A 95% CI for the observed difference was obtained by identifying the 2.5th and 97.5th quantiles of the resulting null distribution. The null hypothesis was rejected if 0 was not included in the 95% CI.
Correction	No correction was performed

Models & analysis

n/a	Involved in the study
☐ ☒	Functional and/or effective connectivity
☒ ☐	Graph analysis
☒ ☐	Multivariate modeling or predictive analysis

Functional and/or effective connectivity   general linear model